© 2015. Published by The Company of Biologists Ltd | Journal of Cell Science (2015) 128, 3569-3582 doi:10.1242/jcs.169094

RESEARCH ARTICLE

Genetic evidence for a microtubule-capture mechanism during polarised growth of *Aspergillus nidulans*

Raphael Manck[1], Yuji Ishitsuka[2], Saturnino Herrero[1], Norio Takeshita[1,3], G. Ulrich Nienhaus[2] and Reinhard Fischer[1,*]

ABSTRACT

The cellular switch from symmetry to polarity in eukaryotes depends on the microtubule (MT) and actin cytoskeletons. In fungi such as *Schizosaccharomyces pombe* or *Aspergillus nidulans*, the MT cytoskeleton determines the sites of actin polymerization through cortical cell-end marker proteins. Here we describe *A. nidulans* MT guidance protein A (MigA) as the first ortholog of the karyogamy protein Kar9 from *Saccharomyces cerevisiae* in filamentous fungi. *A. nidulans* MigA interacts with the cortical ApsA protein and is involved in spindle positioning during mitosis. MigA is also associated with septal and nuclear MT organizing centers (MTOCs). Super-resolution photoactivated localization microscopy (PALM) analyses revealed that MigA is recruited to assembling and retracting MT plus ends in an EbA-dependent manner. MigA is required for MT convergence in hyphal tips and plays a role in correct localization of the cell-end markers TeaA and TeaR. In addition, MigA interacts with a class-V myosin, suggesting that an active mechanism exists to capture MTs and to pull the ends along actin filaments. Hence, the organization of MTs and actin depend on each other, and positive feedback loops ensure robust polar growth.

KEY WORDS: Aspergillus, Polarity, Dynein, Kar9, APC

INTRODUCTION

Polarity establishment and maintenance are essential mechanisms conserved from simple unicellular organisms to higher eukaryotes. Polarity plays an important role in various biological processes, such as embryogenesis, organogenesis, cell morphogenesis and asymmetric cell division. Neurons are among the most polarized cells, and the actin and microtubule (MT) cytoskeletons play essential roles in the correct guidance of axons (Dent et al., 2011).

Simple models for polarized growth are the yeasts *Saccharomyces cerevisiae* and *Schizosaccharomyces pombe*, but also filamentous fungi such as *Aspergillus nidulans* or *Neurospora crassa* (Arkowitz, 2011; Casamayor and Snyder, 2002; Peñalva, 2010; Riquelme, 2013; Takeshita et al., 2014). In filamentous fungi, polarized growth is the dominant growth form and requires continuous extension of the hyphal tip with massive transport of enzymes, and cell wall and plasma membrane components. The actin and MT cytoskeletons, along with their respective motor and other associated proteins, play crucial roles in these transport processes and are also required for establishing and maintaining the polarity axis (Fischer et al., 2008; Takeshita et al., 2014). MTs emerge from spindle pole bodies and septal MTOCs and span the entire hyphae, whereas the actin cytoskeleton is organized very differently (Konzack et al., 2005). Actin patches are found along the hyphae at the cortex, and actin filaments emerge mainly from the hyphal tip and are restricted to a short area behind the tip (Upadhyay and Shaw, 2008). The two cytoskeletons are linked through a class of cortical proteins that are restricted to the apex. They are called cell-end marker proteins and were discovered in *S. pombe* (Snell and Nurse, 1994). Here, one key protein is Mod5, which is prenylated and serves as an anchor for other proteins in the apical membrane (Snaith and Sawin, 2003). It recruits other cell-end marker proteins, such as Tea1 and ultimately the formin For3, which polymerizes actin cables (Feierbach and Chang, 2001). Tea1 is associated with MT plus ends and is delivered through growing MTs (Mata and Nurse, 1997). Hence the MT cytoskeleton organizes the actin cytoskeleton. In *A. nidulans*, cell-end markers are essentially conserved, although sequence similarities are in general very low (Higashitsuji et al., 2009; Takeshita et al., 2008). In contrast to *S. pombe*, MTs converge at one prominent spot at the hyphal tip in *A. nidulans*. This convergence depends on TeaA (Tea1) and TeaR (Mod5) (Takeshita et al., 2008). In addition, it has been shown that the MT polymerase AlpA (XMAP215) interacts with TeaA at the cortex and that polymerase activity is controlled by AlpA (Takeshita et al., 2013). However, the exact mechanism of how MTs converge into a single spot remains unclear. One could hypothesize that growing MTs follow the dome-shaped hyphal apex passively, although this would not explain the observed misguided MTs in the absence of TeaA or TeaR. An alternative mechanism would involve active MT capture and guidance. This hypothesis is based on a model in *S. cerevisiae*.

In *S. cerevisiae*, polarized growth is restricted to a short period of the cell cycle (Martin and Arkowitz, 2014). When the yeast cell forms a daughter bud, the nucleus divides and migrates to the budding neck. This migration depends on astral MTs, which contact the cortex and are subsequently pulled by dynein. In addition to the so-called dynein pathway, a second pathway has been described, which ensures proper spindle alignment and nuclear migration during mitosis (Liakopoulos et al., 2003; Miller and Rose, 1998). The key component of this pathway is Kar9. It localizes initially to the spindle pole body (SPB) but remains only at the SPB that faces the daughter cell. This asymmetry involves multiple phosphorylations of Kar9 by the human CLIP-170 ortholog Bik1 and the Clb4–Cdc28 complex at the SPB, which remains in the mother cell (Liakopoulos et al., 2003; Maekawa et al., 2003; Moore and Miller, 2007; Pereira et al., 2001). After loading Kar9 onto the MT, it is transported to the MT plus end in a Bim1-dependent manner, which classifies Kar9 as a MT-plus-end associated protein

[1]Karlsruhe Institute of Technology (KIT) – South Campus, Institute for Applied Biosciences, Department of Microbiology, Hertzstrasse 16, Karlsruhe D-76187, Germany. [2]Karlsruhe Institute of Technology (KIT) – South Campus, Institute for Applied Physics and Center for Functional Nanostructures, Karlsruhe 76131, Germany. [3]University of Tsukuba, Faculty of Life and Environmental Sciences, Tsukuba, Ibaraki 305-8572, Japan.

*Author for correspondence (reinhard.fischer@kit.edu)

Received 26 January 2015; Accepted 10 August 2015

Journal of Cell Science (2015) 128, 3569-3582 doi:10.1242/jcs.169094

(+TIP) (Akhmanova and Steinmetz, 2010; Liakopoulos et al., 2003; Miller et al., 2000). Once a MT plus end reaches the actin cables, which emerge from the bud tip, Kar9 interacts with the class-V myosin Myo2, which in turn pulls Kar9, the attached MT and the SPB along an actin cable into the daughter cell (Beach et al., 2000; Hwang et al., 2003; Lee et al., 2000; Liakopoulos et al., 2003; Miller et al., 2000; Yin et al., 2000); hence, actin cables guide MTs towards the bud tip.

In this work, we describe MT guiding protein A (MigA) as the first ortholog of Kar9 in filamentous fungi. *A. nidulans* MigA is involved in mitotic spindle positioning, and also in MT capture at the hyphal tip. Furthermore, it is required for cell-end marker positioning and, thereby, for the organization of the MT and actin cytoskeletons during polar growth.

RESULTS

Identification of a Kar9 ortholog in *A. nidulans*

The *A. nidulans* database (www.aspgd.org) was searched for proteins with sequence similarity to *S. cerevisiae* Kar9 (Cerqueira et al., 2013). The best candidate was AN2101, although the similarity was restricted to a short stretch and the Expect (E)-value was only 3×10^{-6} and the overall identity was only 22%. Nevertheless, here we present strong evidence that the two proteins are orthologs. Because the abbreviation *kar* is already used in *A. nidulans*, we named the gene *migA*, referring to the proposed function in MT guidance (see below). The *migA* gene does not contain introns (RNAseq data); the derived protein product comprises 1010 amino acids, with a calculated molecular mass of 109.75 kD and an isoelectric point of 9.01 (Fig. 1A). Analysis using the Pfam database revealed similarities of the region ranging from amino acid 300 to 1004 to the Kar9 protein family, with a bit score of 683.3 and an E-value of 2.4×10^{-205} (Finn et al., 2014). Further analyses revealed other conserved structural features between the two proteins (Fig. 1A). Two putative dimeric coiled-coil domains were identified, one between amino acids 573 and 607, and another one between amino acids 692 and 719, by using the Multicoil algorithm with a maximum search window length of 28 and a P-score of 0.97 and 0.59, respectively (Wolf et al., 1997). Within the alkaline C-terminus of MigA, a SxIP motif (where x is any amino acid) was found at position 873 to 876 (STIP). Such a motif is also present in Kar9, APC and other proteins that are known to bind to end-binding protein 1 (Eb1) and, hence, is a +TIP localization signal (as reviewed by Honnappa et al., 2009). Phosphorylation sites that are essential for asymmetric loading onto SPBs in *S. cerevisiae*, as described by Liakopoulos et al. (2003), were not found in MigA; however, it does possess numerous other predicted phosphorylation sites (data not shown). The MigA protein is well conserved in other filamentous ascomycetes. For instance, *A. nidulans* MigA shares 59% sequence identity with its ortholog in *Penicillium chrysogenum*, and 43% with that in *Neurospora crassa* (Fig. 1B, supplementary material Fig. S1A).

Deletion of *migA* partially phenocopies mutations in cell-end marker genes

To characterize the function of MigA *in vivo*, a *migA*-null mutant was created (Fig. 2A, supplementary material Fig. S2A–C). The *migA* knockout cassette was obtained from the Fungal Genetics Stock Center (Kansas State University, Manhattan, KS) and transformed into the *nkuA*-deletion strain TN02A3. To ensure that the phenotypes are not caused by the *nkuA* deletion, we back-crossed a Δ*migA* strain to an *A. nidulans* wild-type strain (SRF201) and selected a Δ*migA*, *nkuA*$^{+}$ strain. Colonies of all three strains grew as fast as wild-type colonies (Fig. 2A). However, hyphal morphology was affected and resembled the phenotype of mutants lacking the kinesin-VII KipA or cell-end markers, such as TeaA or TeaR (Higashitsuji et al., 2009; Konzack et al., 2005; Takeshita et al., 2008). Deletion mutants lacking TeaA, TeaR or KipA failed to

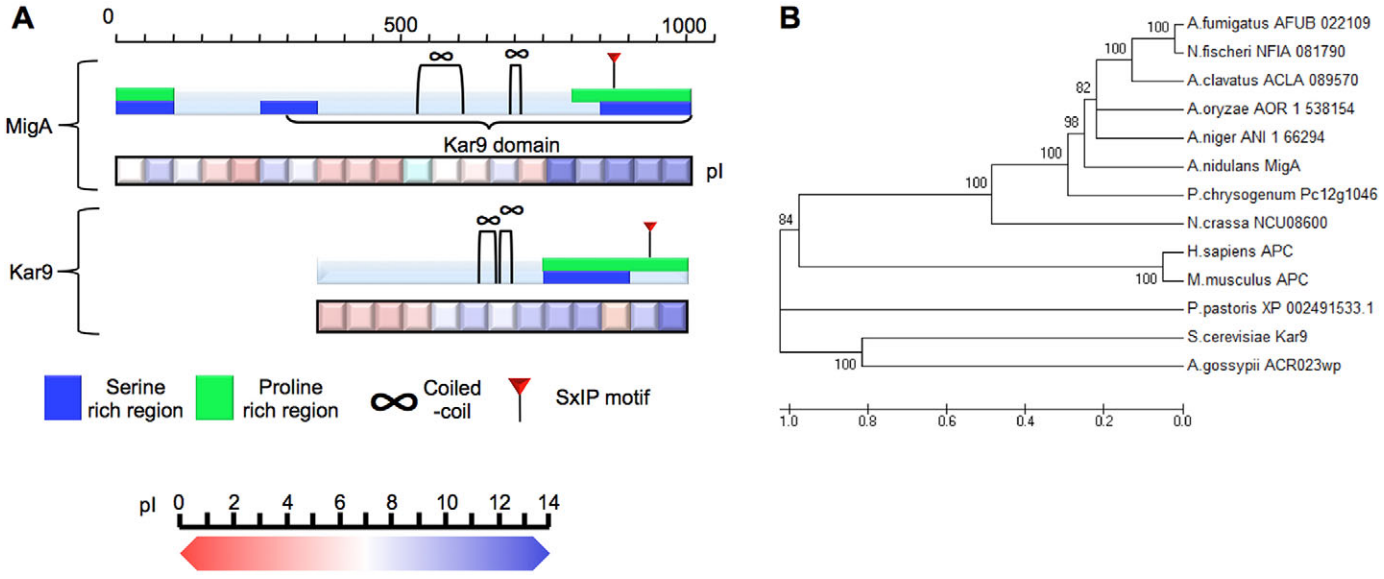

Fig. 1. Scheme of the MigA protein and similarity analysis of MigA orthologs. (A) Comparison of the protein structures of MigA from *A. nidulans* and Kar9 from *S. cerevisiae*. MigA possesses an N-terminal stretch, which is conserved in filamentous fungi. Domains and motifs were determined with Pfam (Finn et al., 2014), Protparam (Gasteiger et al., 2005) and MultiCoil (Wolf et al., 1997). Furthermore, domains and motifs of Kar9 are indicated as described previously (Liakopoulos et al., 2003, Miller and Rose, 1998). (B) MigA groups together with putative orthologs of other *Aspergilli* and filamentous fungi. Putative orthologs were identified using a blastp search with the full-length protein sequence of MigA as the query sequence (Altschul et al., 1990). The alignment was performed with CLC Sequence Viewer 6.6.1 (Qiagen, Venlo, The Netherlands) (gap open cost, 10.0; gap extension cost, 1.0) and a phylogenetic tree was created with a neighbor-joining algorithm and bootstrapping analysis (replicates, 100) using MEGA5.2 (Tamura et al., 2011).

Journal of Cell Science (2015) 128, 3569-3582 doi:10.1242/jcs.169094

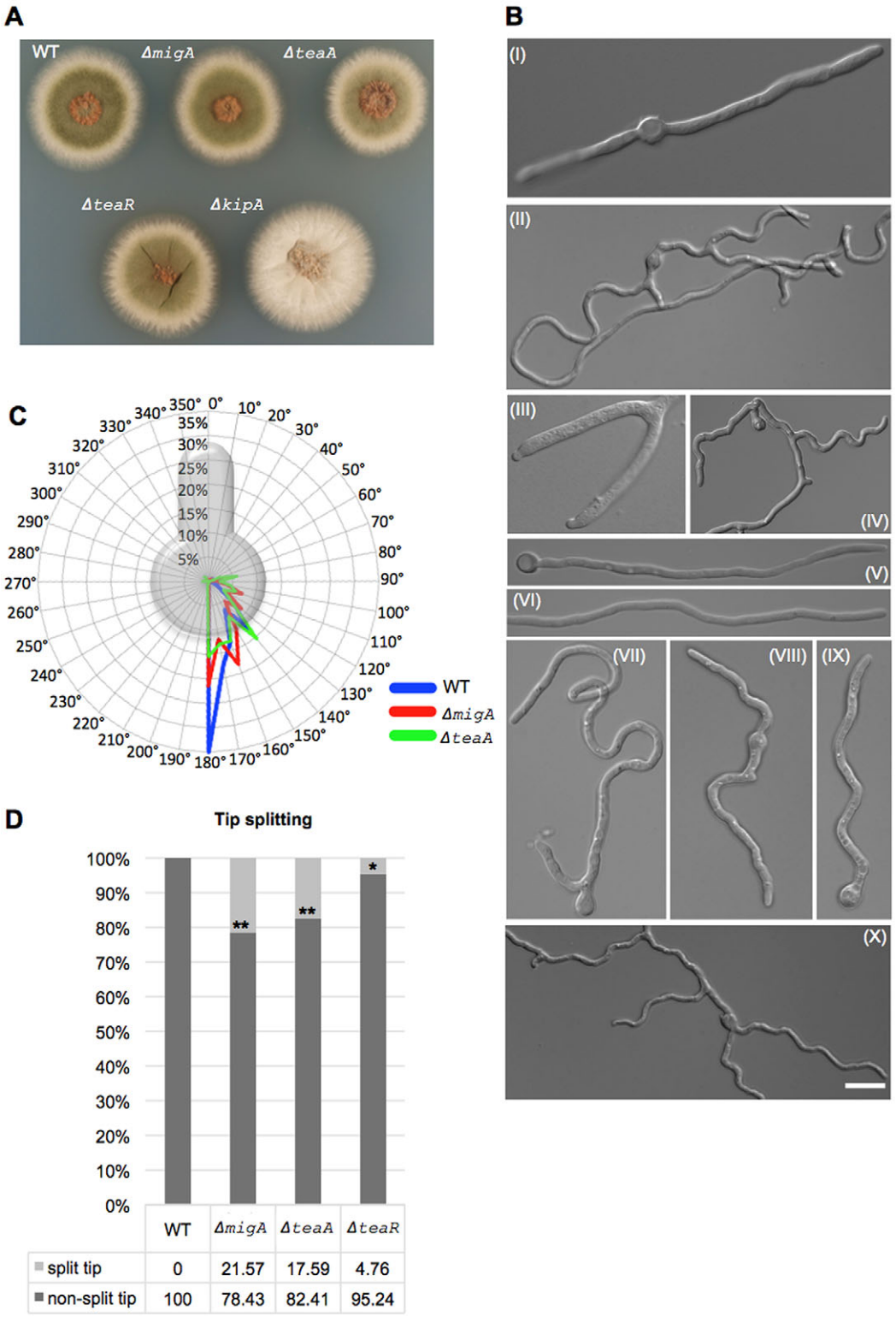

Fig. 2. See next page for legend.

maintain the internal polarity axis, resulting in curved or zig-zag growth patterns, which was most apparent in medium with 2% glucose as the carbon source. Furthermore, tip splitting could be observed (Fig. 2A,B,D). In addition, polarity establishment, as required during the germination of conidiospores, was affected. The angle of emerging secondary hyphae was significantly different from that in wild type, and a third germ tube occurred more frequently. This resembled the effects of loss of the cell-end marker TeaA (Fig. 2B,C).

MigA localizes to mitotic spindles and facilitates contact between astral MTs and cortical ApsA

To determine the localization of MigA, enhanced green fluorescent protein (GFP) was fused to the C-terminus of MigA and expressed

Journal of Cell Science (2015) 128, 3569-3582 doi:10.1242/jcs.169094

Fig. 2. Phenotypic analysis of a *migA*-deletion strain. (A) Colonies of wild-type (WT, SRF201), Δ*migA* (SRM11), Δ*teaA* (SRM127), Δ*teaR* (SNT34) and Δ*kipA* (SSK44) strains. Strains were grown on Minimal Medium (MM) agar plates supplemented with appropriate vitamins and 2% glucose for 3 days at 37°C. (B) Hyphae of wild-type (I) (TN02A3), Δ*migA* (II, III) (SRM11), *migA* under $alcA_{(p)}$ control (SRM12) and repressed with 2% glucose (IV), derepressed with 2% glycerol (V), or induced with 2% threonine and 0.01% glucose (VI), Δ*teaR* (VII) (SNT34), Δ*teaA* (VIII) (SRM127), Δ*kipA* (IX) (SSK44) and Δ*teaA*/Δ*migA* (X) (SRM117). Strains were grown as described with 2% glucose or as indicated. Scale bar: 5 µm (I, III); 10 µm (II,IV–VI, X); 8 µm (VI–IX). (C) Quantification of the impact of a *migA* deletion on second germ tube formation. Because the normal distribution of the data is not given (as determined using a Kolmogoroff–Smirnoff and chi-squared test), a Mann–Whitney U test was applied. Germ tube emergence was significantly altered in Δ*migA* (P=0.00298) and Δ*teaA* (P=0.00038) strains compared to the wild type at $P \leq 0.01$. However, emergence did not differ significantly (P=0.16152) between Δ*migA* and Δ*teaA* strains [$n_{(WT)}$=120, mean=153.74±25.28; $n_{(\Delta migA)}$=143, mean=145.27±34.65; $n_{(\Delta teaA)}$=84, mean=141.15±41.75]. Conidia of wild type (SRF201), Δ*migA* (SRM11) and Δ*teaA* (SRM127) strains were grown as described, and the angle of emergence of a second germ tube in relation the first one was measured. The acquired data sets were sorted in 10° groups and plotted in a radar plot. (D) Quantification of tip-splitting events in wild-type, Δ*migA*, Δ*teaA* and Δ*teaR* strains. Tip splitting events in Δ*migA* (P=0) and Δ*teaA* (P=0) strains were significantly higher in comparison to the wild type at P<0.01, whereas in Δ*teaR* (P=0.024) strains, it only differed at P<0.05. By contrast, the number of split tips between Δ*migA* and Δ*teaA* (P=0.47) did not differ significantly at P<0.1. However, Δ*teaR* differed significantly from Δ*migA* (P=0.0003) and Δ*teaA* (P=0.003) at P<0.1. In comparison to the wild type, where no tip splitting was observed, the occurrence of this event in Δ*migA* (21.57%), Δ*teaA* (17.59%) and Δ*teaR* (4.76%) strains was significantly higher [wild type, $n_{(cells)}$=104; Δ*migA*: $n_{(cells)}$=102; Δ*teaA*: $n_{(cells)}$=108; Δ*teaR*: $n_{(cells)}$=10]. Conidia of wild type (SRF201), Δ*migA* (SRM11), Δ*teaA* (SRM127) and Δ*teaR* (SNT34) strains were grown as described on 2% glucose agar plates and screened for tip-splitting events at the periphery of the colony. *$P \leq 0.01$; **$P \leq 0.1$; ± is s.d.

under the control of the endogenous promoter. MigA–eGFP localized along the mitotic spindle, including SPBs (Fig. 3A). In addition, a small cluster was found at septa (data not shown). This suggests that MigA is present at septal and nuclear MTOCs. The localization of the protein appeared to be very dynamic, and the signal intensities at the SPBs changed over time before they appeared at astral MTs (Fig. 3A, supplementary material Movie 1). When cells were treated with benomyl, MigA localized in clusters at the plasma membrane (supplementary material Fig. S3A). To test whether MigA interacts with the cortical protein ApsA (Fig. 3D, supplementary material Fig. S3B) (Fischer and Timberlake, 1995) in the same fashion that *S. cerevisiae* Kar9 interacts with Num1 (Farkasovsky and Kuntzel, 2001), bimolecular fluorescence complementation (BiFC) and yeast two-hybrid analyses were performed. BiFC analysis showed an interaction of the two proteins at the plasma membrane throughout the fungal hyphae and also occasionally at septa (Fig. 3B). Because false-positive results can be obtained in a BiFC analysis (Kerppola, 2008), we performed additional BiFC experiments with MT-associated proteins such as KipA and AlpA, and the cell-end markers TeaR and TeaC. No signals were obtained in any of the combinations with MigA (data not shown). The yeast two-hybrid assay indicated that MigA interacts with the N-terminal part of ApsA under medium stringency conditions (Fig. 3C). As a negative control, the MigA–TeaR interaction was included (Fig. 3C).

Because spindle motility in *apsA*-deletion strains is nearly abolished, we analyzed this phenotype in a Δ*migA* strain and compared it to the Δ*apsA* strain. In both cases, spindle motility was significantly reduced in comparison to that of the wild type, although the effect was stronger in the absence of ApsA (Fig. 3E). In the *migA*-deletion strain, astral MTs failed to make contact with the cortex in early stages of mitosis (supplementary material Movie 2), and thus we reasoned that MigA, like Kar9 in *S. cerevisiae*, has a role in positioning of the nucleus during the early stages of mitosis. This is consistent with the fact that Δ*migA* strains do not show a nuclear misdistribution phenotype, whereas Δ*apsA* strains do (Fig. 3F).

MigA associates with growing and retracting MT plus ends in an EbA-dependent manner

Time-lapse analyses of MigA–eGFP revealed that it is transported to the hyphal tip in interphase cells (Fig. 4A–C). This behavior resembles that of the MT-plus-end-associated motor protein KipA. The velocity of KipA is 9.5±1.8 µm/min (Schunck et al., 2011), whereas the growth rate of MT is 13.7±3.1 µm/min (Han et al., 2001). MigA comets were imaged *in vivo*, and velocities of 11.9±9.5 µm/min were calculated, thus resembling the velocities of KipA and growing MTs (Fig. 4C). Dual labeling of TubA and MigA revealed that MigA is loaded onto the SPBs and, from there, actively transported towards the MT plus end (Fig. 4B, supplementary material Movie 3). Overexpression of eGFP–MigA led to complete decoration of cytoplasmic MTs (supplementary material Fig. S4A, Movie 4). In addition to eGFP fusions, we generated a fusion with photoconvertible mEosFPthermo (Wiedenmann et al., 2004, 2011), which allows for analysis using super-resolution microscopy, such as photoactivated localization microscopy (PALM; for a review of super-resolution microscopy, see Patterson et al., 2010). Super-resolution single-particle-tracking analysis of MigA–mEosFPthermo (MigA tagged at the C-terminus) clusters provided essentially background-free images and showed localization of single MigA clusters at growing and retracting MTs (Fig. 4D, supplementary material Movie 5).

Furthermore, we investigated the potential roles of the Kar9 domain and the conserved N-terminal stretch of MigA. Deletion of the N-terminal stretch did not alter the localization and dynamics of the protein, whereas deletion of the Kar9 domain affected both. The corresponding protein was observed mainly in the cytoplasm and as accumulations in a subapical region that resembled the endocytic collar (Fig. 4E,F). Thus, the Kar9 domain is required for association with MTs.

In order to test whether MT plus end association of MigA depends on the *A. nidulans* Eb1 ortholog EbA (Zeng et al., 2014), BiFC assays were performed to determine whether they interact. A strong signal along short and long filamentous structures was observed in hyphae. The features observed in the images resembled MTs, which suggests that MigA and EbA interact at the MT lattice (Fig. 5A). Other MT-associated proteins, such as KipA and AlpA, did not interact with MigA (data not shown) (Enke et al., 2007; Zekert and Fischer, 2009). The EbA–MigA interaction was confirmed in a yeast two-hybrid assay (Fig. 5B). The predicted SxIP motif at position 873–876 in MigA was not essential for the MigA–EbA interaction (Fig. 5B). Surprisingly, the SxIP domain was crucial for the transport of MigA *in vivo* and accumulated in non-motile clusters in the hyphae (Fig. 5C).

In order to address the question whether MigA is loaded onto MT in an EbA-dependent manner, we analyzed MigA–eGFP in a Δ*ebA*-deletion strain. In contrast to KipA (Zeng et al., 2014), for example, MigA still localized to MTs. However, MTs were more uniformly decorated, and MT plus end accumulation was abolished, although this did not completely phenocopy a deletion of the SxIP motif (Fig. 5C–E). We also observed MigA at septa and uniformly decorated mitotic spindles (data not shown), suggesting EbA-independent binding of MigA to septa, mitotic spindles, SPBs and MTs. Direct interaction of MigA and TubA was further proven with

Journal of Cell Science (2015) 128, 3569-3582 doi:10.1242/jcs.169094

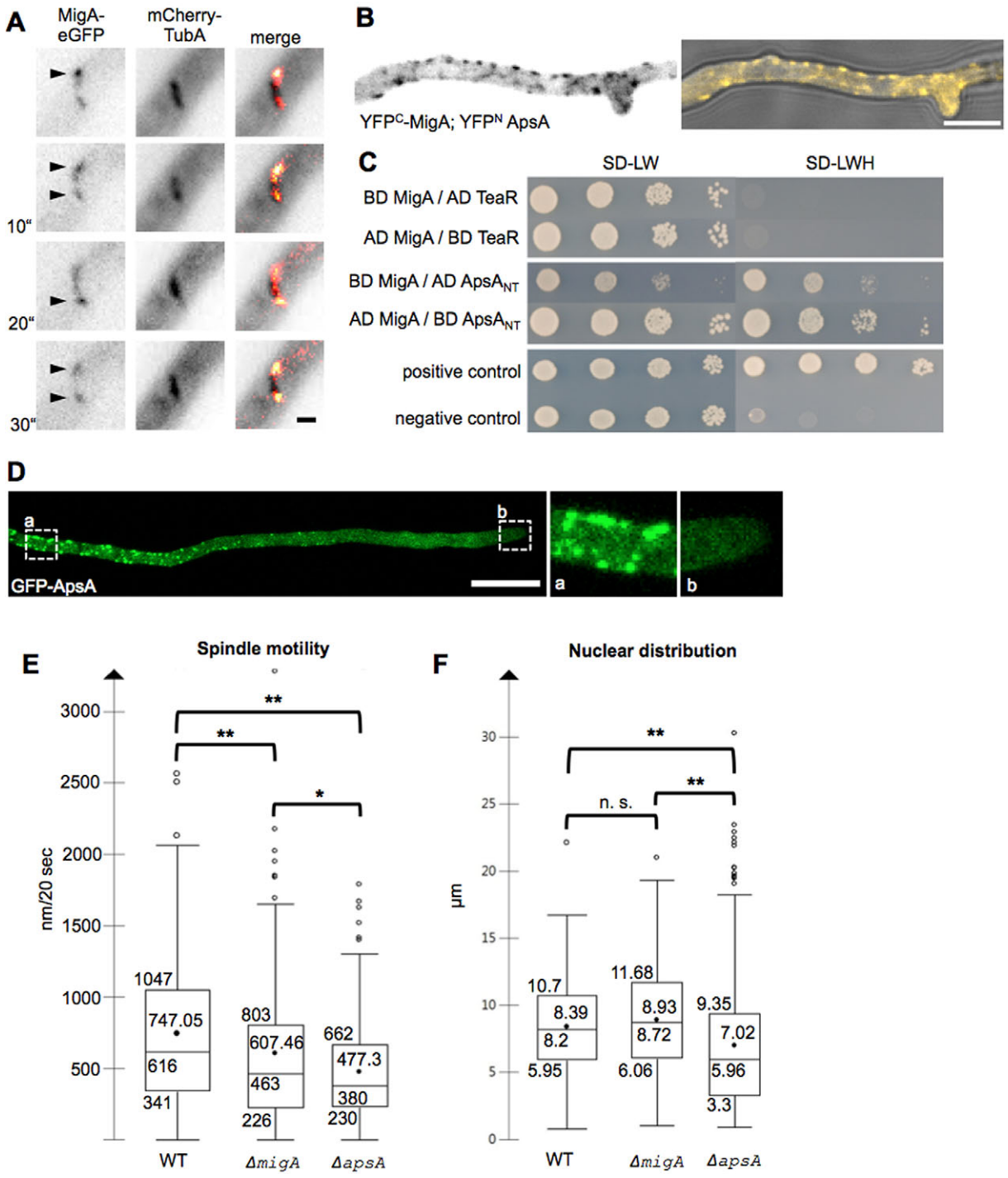

Fig. 3. See next page for legend.

BiFC and yeast two-hybrid assays (Fig. 5B,F). In this series of experiments, strong self-interaction of MigA was observed in the yeast two-hybrid assay (Fig. 5B).

MigA plays a role in cell-end marker positioning and MT convergence

Because the phenotype of Δ*migA* strains resembled that of null mutations of cell-end marker mutants, we anticipated that MigA is involved in cell-end marker positioning. To test this, tagged cell-end markers eGFP–TeaR (N-terminally tagged) and mRFP1.2–TeaA, expressed from their natural promoters, were analyzed in Δ*migA* and wild-type strains (Fig. 6A). Indeed, the number of hyphae with mis-positioned TeaA or TeaR was higher than in wild type. Next, we analyzed the direct interaction of MigA with cell-end marker proteins using the BiFC and yeast two-hybrid assays. TeaA did interact, whereas TeaC and TeaR did not (Fig. 6B,C, Fig. 3C; BiFC assay, data for MigA–TeaC and MigA–TeaR interactions are not shown). The interaction of MigA and TeaA was restricted to the hyphal tip, and occasionally to septa. We did not observe transport of any assembled BiFC complexes, which suggests that the interaction only takes place at the tip. Furthermore, we observed a strong dominant-negative phenotype on polarized growth in these

Journal of Cell Science (2015) 128, 3569-3582 doi:10.1242/jcs.169094

Fig. 3. Localization of MigA and its role in mitotic spindle dynamics. (A) Dynamic localization of MigA–eGFP at both spindle poles (arrowheads), along the mitotic spindle and on astral MTs. Hyphae of SRM22 (*migA::eGFP*, $alcA_{(p)}$*::mCherry::tubA*) were grown as described (exposure times 450–490 nm, 500 ms; 538–562 nm, 500 ms). Scale bar: 1 µm. (B) Confocal scanning image of the interaction of MigA and ApsA at the hyphal membrane. Hyphae of the strain SRM14 ($alcA_{(p)}$*::YFPC::migA*, $alcA_{(p)}$*::YFPN::apsA*) were grown as described (frame accumulation, 2; line average, 16; AOTF 514, 25%; gain, 900 V; offset, –0.2; scan speed, 1000 Hz; emission bandwidth, 522 nm–648 nm; maximum projection of a 5.16 µm *z*-stack). Scale bar: 5 µm. (C) Yeast two-hybrid analysis of MigA and ApsA. Strains expressing different versions of MigA and TeaR served as controls. Positive and negative controls as provided in the Matchmaker™ Gold Yeast Two-Hybrid System by Clontech Laboratories. Dilution series of respective strains were grown on selective dropout leucine and tryptophan medium (SD-LW) and selective dropout leucine, tryptophan and histidine (SD-LWH) at 30°C for 3 days. AD, activating domain; BD, binding domain. (D) Confocal scanning image of the localization of ApsA in distal parts of the hyphae (a). ApsA does not localize to hyphal tips (b). Hyphae of the strain SRM176 ($alcA_{(p)}$*::eGFP::apsA*) were grown as described (frame accumulation, 2; line average, 4; AOTF 488, 5%; gain, 900 V; offset, –0.1; scan speed, 400 Hz; emission bandwidth, 492 nm–652 nm; maximum projection of a 6.29 µm *z*-stack). Scale bar: 10 µm. (E) Boxplot of spindle motility analysis of wild-type (WT, SRM118), Δ*migA* (SRM124) and Δ*apsA* (SRM136). The respective strains were grown as described, and time-lapse images were taken from mitotic spindles every 4 s (exposure time 450–490 nm, 50 ms). Distance of the spindle movement was measured every frame until the end of mitosis or loss of fluorescence. Measured distances were grouped into 20-s intervals and plotted. Because the normal distribution of the data is not given (as determined using a Kolmogoroff–Smirnoff and chi-squared test), a Mann–Whitney U test was applied. The boxplot was created with Boxplot 1.0.0 (8). Spindle motility was significantly altered in Δ*migA* (P=0.00496) and Δ*apsA* (P=0) strains compared to the wild type at $P \leq 0.01$. However, emergence only differed significantly (P=0.0703) between Δ*migA* and Δ*apsA* strains at $P \leq 0.1$. [Wild type, $n_{(cells)}$=22, $n_{(spindle)}$=29, $n_{(data\ points)}$=142; Δ*migA*, $n_{(cells)}$=15, $n_{(spindle)}$=20, $n_{(data\ points)}$=151; Δ*apsA*, $n_{(cells)}$=13, $n_{(spindle)}$=29, $n_{(data\ points)}$=190]. *$P \leq 0.01$; **$P \leq 0.1$. (F) Boxplot of nuclear distribution analysis of wild type (SRM118), Δ*migA* (SRM124) and Δ*apsA* (SRM136). The respective strains were grown as described, and nuclei stained with DAPI (Vector Laboratories, Vectashield Mounting Medium with DAPI, number H-1200), and the distance between neighboring nuclei was measured. Because the normal distribution of the data is not given (as determined using a Kolmogoroff–Smirnoff and chi-squared test), a Mann–Whitney U test was applied. The boxplot was created with Boxplot 1.0.0 (8). Nuclear distribution was significantly altered in Δ*apsA* strains compared to the wild type ($P<2\times10^{-06}$) and Δ*migA* ($P<2.2\times10^{-06}$) at $P<0.001$. Nuclear distribution between the wild-type and Δ*migA* strains did not differ significantly (P=0.089) at $P \geq 0.05$. [Wild type, $n_{(cells)}$=32, $n_{(nuclei)}$=336; Δ*migA*, $n_{(cells)}$=31, $n_{(nuclei)}$=337; Δ*apsA*, $n_{(cells)}$=30, $n_{(nuclei)}$=396]. In the boxplots, the line represents the median, the boxes represent all data points between the 75% and 25% quantile, and the whiskers represent the maximum and minimum values. **$P \leq 0.001$. n.s., not significant; NT, N-terminal.

strains, where hyphae displayed meandering growth, similar to that of the *migA teaA* double-deletion strain (Fig. 2B). The observed phenotypes were not due to the tagging of MigA or TeaA with the split yellow fluorescent protein (YFP) halves (supplementary material Fig. S4B). As inferred from the interaction of MigA with TeaA, MT convergence in the hyphal tip was affected in Δ*migA* as in Δ*teaA* strains (Fig. 6D, supplementary material Movie 6).

The interaction between MigA and MyoE provides an active guidance mechanism for MTs along actin filaments

A possible mechanism for MT convergence in the hyphal tip is active pulling of the MT plus ends along actin cables that originate from the cell-end marker complex. To test this hypothesis, we examined an interaction of MigA with the class-V myosin MyoE (MyoV), which localizes *in vivo* to the hyphal tip and associates with secretory vesicles (Taheri-Talesh et al., 2012; Zhang et al., 2011). BiFC analysis revealed a strong fluorescence signal at the hyphal tip and along some filamentous structures originating from the cortex (Fig. 7A). Strains overexpressing *migA* displayed a slightly curvy phenotype and no difference in the phenotype at the colony level, whereas hyphae in *myoE*-overexpressing strains were considerably thicker and showed a growth defect on solid medium (supplementary material Fig. S4A,C,E). The corresponding BiFC strain also showed strong growth defects with smaller colonies and a defect in spore formation, and the diameter of hyphae gradually increased from the spore to the tip (supplementary material Fig. S4D,E). The phenotype of the BiFC strain also resembled a *myoE*-deletion phenotype, which suggests that MyoE is not functional, probably owing to the irreversible interaction of the two split YFP halves. Thus, *in vivo*, the interaction can only be transient. The interaction between MigA and MyoE was further confirmed in a yeast two-hybrid assay (Fig. 7B).

Colocalization studies with eGFP-tagged MigA and mCherry-tagged MyoE should show co-transport of both proteins. However, the MyoE concentration – even after expression under its native promoter – is too high to resolve such co-transport (Taheri-Talesh et al., 2012). In order to lower the concentration of the tagged MyoE protein, we generated a strain with mCherry-tagged MyoE, which has a modified stop codon (TGACTA) between the coding sequence of *myoE* and *mCherry*. This stop codon has been shown to frequently trigger translational readthrough (Freitag et al., 2012; Stiebler et al., 2014). In this strain, only a small fraction of MyoE was labeled with mCherry and this allowed tracking of smaller clusters of MyoE at the tip. Using this construct, we observed partial colocalization of MigA and MyoE in the tip (Fig. 7C). Despite being almost below the detection limit, meaning that time resolution was challenging, we were able to detect co-transport of both proteins at the hyphal tip (supplementary material Movie 7). In the corresponding time-lapse series, signals of MyoE moved away from the tip and returned together with MigA comets (supplementary material Movie 7).

DISCUSSION

The interaction and attachment of MTs to chromosomal kinetochores, and the temporal interaction of MTs with defined cortical regions during polarized cellular extension are two prominent examples of the necessity of MT capture in eukaryotic cells (Carminati and Stearns, 1997; Fodde et al., 2001; Reilein et al., 2005; Lu et al., 2001). The mechanisms require the spatial and temporal interaction between MT-plus-end-associated proteins and target protein complexes, which transmit information to downstream processes. If only a small number of MT-plus-end-associated proteins (or only one) were required for different MT interactions, one would assume that the specificity also relies on different interacting proteins. Here, we found that the +TIP protein MigA is able to interact with two cortical proteins, ApsA and TeaA. The downstream processes are very different, however, for the two cases. The interaction with ApsA promotes spindle oscillations and is most likely to involve the activation of the dynein pathway as in *S. cerevisiae*, whereas dynein is not activated upon interaction with the cell-end marker protein TeaA. The two processes are spatially separated because ApsA does not reach the hyphal tip, whereas TeaA is restricted to the hyphal tip (Fig. 3D, supplementary material Fig. S4F).

The interaction of MigA with ApsA is conserved in relation to that in *S. cerevisiae*. However, nuclear division in yeast is correlated with nuclear migration and asymmetric movement of the dividing nucleus into the bud neck. This asymmetry is generated, in the first instance, by asymmetric loading of Kar9 onto the two SPBs. Such asymmetry is not required in vegetative hyphae of filamentous

Journal of Cell Science (2015) 128, 3569-3582 doi:10.1242/jcs.169094

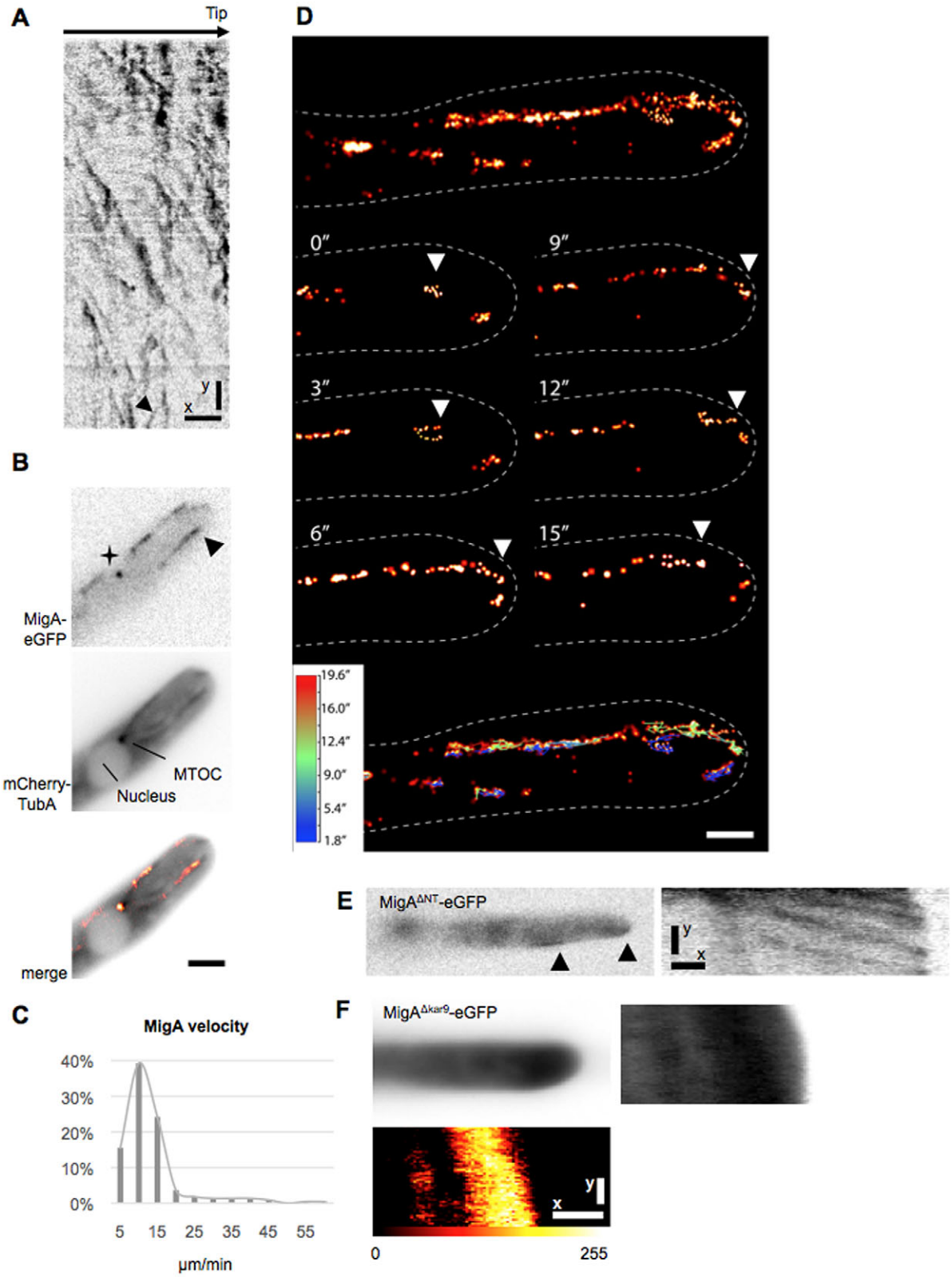

Fig. 4. See next page for legend.

fungi because interphase nuclei migrate within the hyphae (Suelmann et al., 1998). Nevertheless, the dynamic behavior of Kar9 appears to be conserved in MigA. When the MigA concentration increased at one SPB, it decreased at the other. This oscillation was repeated several times during mitosis. Such fluctuations of MigA came as a surprise because, in *S. cerevisiae*, asymmetric loading of Kar9 results from phosphorylation of a number of serine residues (Liakopoulos et al., 2003). However,

Journal of Cell Science (2015) 128, 3569-3582 doi:10.1242/jcs.169094

Fig. 4. Localization of MigA at growing and retracting MT plus ends. (A) Kymograph of MigA–GFP comets traveling towards the tip. Retrograde movement can also be observed (arrowhead). Hyphae of SRM1 (*migA::eGFP*) were grown as described (exposure times 450–490 nm, 500 ms). Scale bars: 1 µm (*x*); 20 s (*y*). (B) MigA binds to MTOCs (♠) at the nucleus and is transported to the MT plus ends (arrowhead). Hyphae of the strain SRM22 (*migA::eGFP*, $alcA_{(p)}$*::mCherry::tubA*) were grown as described (exposure time 450–490 nm, 500 ms; 538–562 nm, 500 ms). Scale bar: 2 µm. (C) Velocity of MigA–GFP comets *in vivo*. Calculated mean velocity ± s.d. is 11.91±9.49 µm/min [$n_{(cells)}$=8; $n_{(MigA\ signals)}$=219; time-lapse sequences lasting a total of 1272 s]. 63.47% of the measured velocities were between 5 and 15 µm/min. Hyphae of SRM1 (*migA::eGFP*) were grown as described, and time-lapse images were taken (exposure times 450–490 nm, 500 ms). Velocities were measured using kymographs. Measured velocities were grouped and plotted. (D) Analyzed positions of mEosFPthermo-labeled MigA molecules from PALM single-particle-tracking analysis. Snapshots taken from an 18-s time-lapse image (total imaging time). Images show the maximum projection of 16 individual images acquired during each 3.3-s interval. Overlay shows the computed positions of all MigA–mEosFPthermo clusters detected in the time-lapse image. MigA localizes to growing and retracting MT plus ends (arrowheads). Lines shown in the bottom image indicate trajectories of individual MigA clusters, and colors indicate different initial times of the trajectories. Hyphae of the strain SRM40 (*migA::mEosFPthermo*, $alcA_{(p)}$*::eGFP::tubA*) were grown as described (exposure time 200 ms). Scale bar: 1 µm. (E) $MigA^{\Delta NT}$ (arrowheads) comets move towards the tip of the hyphae. Hyphae of SRM199 ($migA^{\Delta NT}$*::eGFP*) were grown as described, and time-lapse images were taken (exposure times 450–490 nm, 800 ms). Scale bars: 2 µm (*x*); 15 s (*y*). (F) $MigA^{\Delta kar9}$ localizes to the cytoplasm and also accumulates in a subapical region (maximum projection of a 100-s time-lapse image). Hyphae of SRM198 ($migA^{\Delta kar9}$*::eGFP*) were grown as described, and time-lapse images were taken (exposure times 450–490 nm, 800 ms). Scale bars: 2 µm (*x*); 25 s (*y*). False color heat map (bottom) shows fluorescence intensities as color scheme. NT, N-terminus.

because these serine residues are not conserved in MigA, a different mechanism is likely to play a role. In any case, the fluctuations themselves reveal the potential for stable asymmetric loading of MigA onto the SPBs. This might be of importance during mitotic events in conidiophore development. The formation of primary and secondary sterigmata, indeed, closely resembles the budding process in *S. cerevisiae*. Without MigA, astral MTs fail to establish contact with the plasma membrane and/or ApsA and retract. As in *S. cerevisiae*, where the Kar9 pathway is predominantly active during pre-anaphase, MigA is important in nuclear positioning during the early stages of mitosis, because in later stages of mitosis, astral MTs are able to establish contact with the cortex (supplementary material Movie 2). Following the yeast model (Miller and Rose, 1998; Liakopoulos et al., 2003), the MigA and dynein pathways are partially redundant, and therefore, dynein can fulfill the functions of MigA. This is consistent with our observation that distribution of the nuclei was not significantly altered in a Δ*migA* strain (Fig. 3F). This leads to the suggestion that MigA is not essential for the binding of astral MTs to cortex proteins, such as ApsA, but instead is a promoting factor that facilitates contact between ApsA and astral MTs (Fig. 8A, supplementary material Movie 2).

In interphase cells, MigA is actively transported to the hyphal tip. This transport is dependent on the Eb1 ortholog EbA (Fig. 5A–E), although MigA is able to bind to α-Tubulin (TubA) autonomously (Fig. 5B,F). In a yeast two-hybrid screen, the SxIP motif that had been identified *in silico* in the C-terminus of MigA turned out to not be essential for the interaction of the two proteins. It is not unusual for Eb1 interaction partners to harbor more than one and/or degenerated SxIP motifs, or alternatively MT plus end and/or Eb1-binding sites that do not match the SxIP consensus sequence (van der Vaart et al., 2011). However, the SxIP motif was crucial for MigA motility (Fig. 5C). Surprisingly, deletion of the SxIP did not completely phenocopy deletion of *ebA*.

The key novel finding in this work is that MigA is able to transiently interact with the cell-end marker protein TeaA. Apparently, MigA plays a role in correct positioning of TeaA. This might be explained by a MT capture mechanism in the hyphal tip (Fig. 7C, Fig. 8B, supplementary material Movie 7). The interaction of MigA with TeaA would ensure docking of the MT plus end to the TeaA protein complex. The establishment of such a complex involves a positive-feedback loop. Initially, only a few molecules of TeaA are delivered to one position at the cortex. From there, some actin cables are launched, which in turn guide more MT plus ends (through the action of MigA and MyoE) to this spot and, thus, again increase the TeaA concentration (N. Takeshita, Karlsruhe, personal communication). Another possible explanation for the guidance mechanism of the MT plus ends along actin cables could be a bridging of the two cytoskeletons by secretion vesicles, which are associated with both kinesin and MyoE (Pantazopoulou et al., 2014). However, this mechanism would not explain why deletion of *migA* affects MT convergence in the hyphal tip.

Another explanation for the interaction between TeaA and MigA could be regulation of TeaA. TeaA interacts with the MT polymerase AlpA and controls its activity (Takeshita et al., 2013). However, both TeaA and AlpA are transported to the MT plus end, and we have no evidence that they interact there. It would actually be very disadvantageous if TeaA were to interact with AlpA at the MT plus end because this could lead to inactivation of AlpA activity, which is proposed to happen only at the cortex. MigA also appears to interact only at the hyphal tip with TeaA, and this interaction could change the activity of AlpA. TeaA thus appears to be a scaffold protein that is engaged in stable interactions with proteins such as TeaR or TeaC, and also transient interactions with proteins such as MigA or AlpA. In *S. cerevisiae*, it has not yet been reported that Kar9 interacts with the TeaA ortholog Kel1. However, cell-end marker proteins (landmark proteins) in *S. cerevisiae* do not play a direct role in polarized growth. Cells lacking *kel1* are defective in cell fusion during mating owing to failure of membrane fusion and cytoplasmic mixing. By contrast, cells lacking the *kel1* paralog *kel2* do not show any abnormal phenotype during cell fusion (Philips and Herskowitz, 1998). Given the high conservation of MigA and its long N-terminal extension in all analyzed filamentous ascomycetes, the proposed mechanism of MT capture in the hyphal tip might be a newly identified evolutionary function, which contributes to the understanding of the mechanism of polar growth in filamentous fungi.

The ortholog of MigA, Kar9, is frequently referred to as the functional ortholog of the human adenomatous-polyposis-poli (APC) protein in *S. cerevisiae* (Liakopoulos et al., 2003; Miller and Rose, 1998). Although Kar9 possesses only a short amino acid sequence that is similar to APC, it might share some functions with APC (Bloom, 2000). APC is an extensively studied tumor suppressor with a well-known role in the (canonical) Wnt signaling pathway, where APC is part of a protein complex that triggers degradation of β-catenin (Behrens et al., 1998; Groden et al., 1991). In neuronal tissue, however, APC plays another important role, and the MT and actin cytoskeletons are highly disturbed if APC is missing (Chen et al., 2011). It has been shown that APC contains a functional MT-binding site at the C-terminus, which can stimulate MT assembly as well as bundling *in vitro*, and stabilize MTs *in vitro* and *in vivo* (Munemitsu et al., 1994; Zumbrunn et al., 2001).

Eb1 is an important interaction partner of APC that was discovered in a yeast two-hybrid screen using APC as bait

Journal of Cell Science (2015) 128, 3569-3582 doi:10.1242/jcs.169094

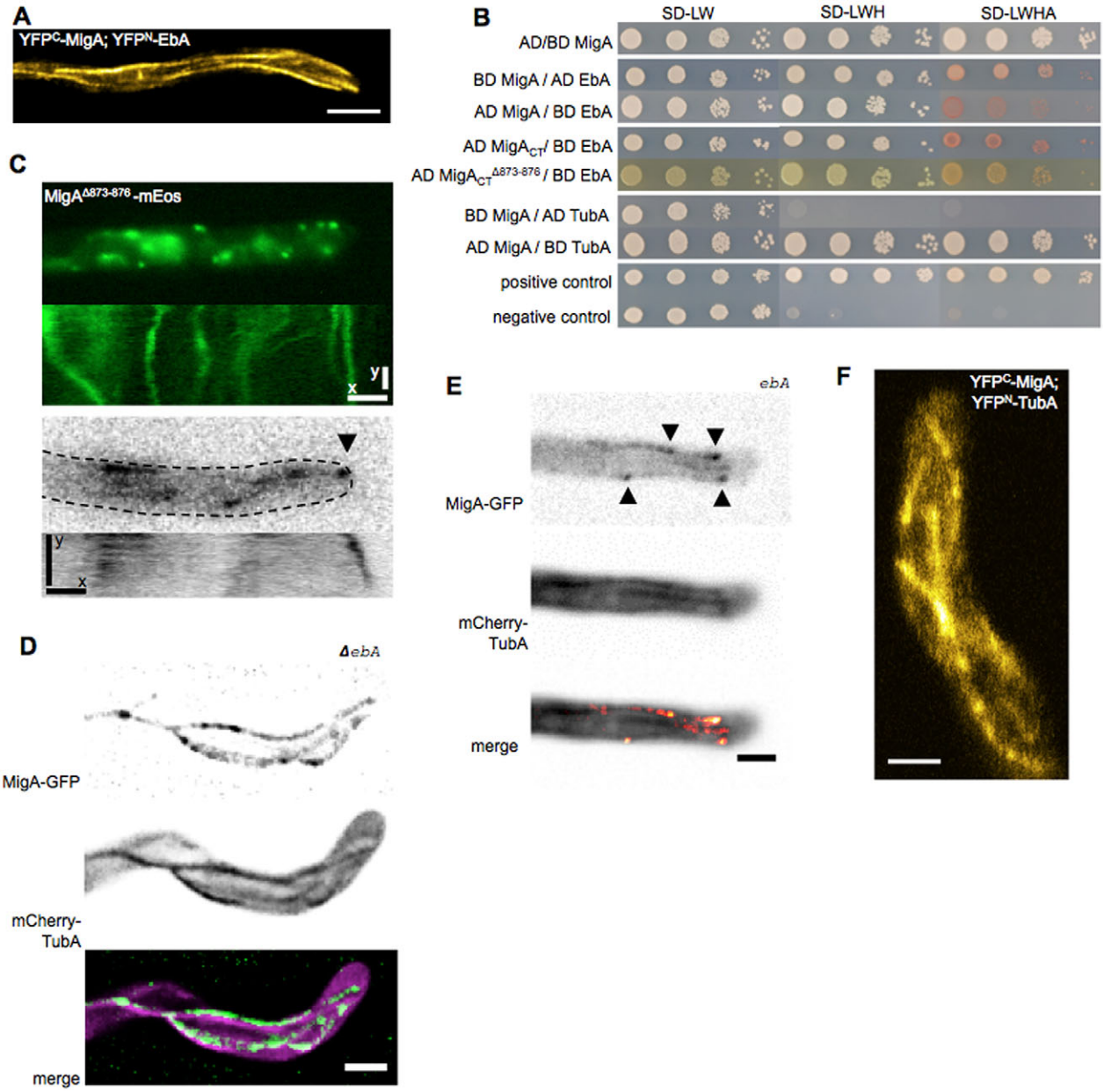

Fig. 5. Interaction of MigA with EbA and TubA. (A) Confocal scanning image of the BiFC of MigA and EbA at filamentous structures. Hyphae of the strain SRM105 (*alcA$_{(p)}$::YFPC::migA*, *alcA$_{(p)}$::YFPN::ebA*) were grown as described (line average, 128; AOTF 514, 10%; gain, 1000 V; offset, –0.2; emission bandwidth, 522 nm–658 nm); scale bar: 5 µm. (B) Yeast two-hybrid analysis of MigA and EbA, TubA. Positive and negative controls as provided in the Matchmaker™ Gold Yeast Two-Hybrid System by Clontech Laboratories. Dilution series of respective strains were grown on selective dropout leucine and tryptophan (SD-LW), selective dropout leucine, tryptophan and histidine (SD-LWH) and selective dropout leucine, tryptophan, histidine and alanine (SD-LWHA) at 30°C for 3 days. (C) MigA$^{\Delta 873–876}$ localizes to cytoplasmic clusters and also accumulates at the hyphal tip (arrowhead). Motility of these clusters was impaired in comparison to wild-type MigA. Hyphae of SRM201 (*migA$^{\Delta 873–876}$::mEosFPthermo*) were grown as described, and time-lapse images were taken (exposure times 450–490 nm, 500 ms). Kymograph shows motility of MigA$^{\Delta 873–876}$. Scale bars: 2 µm (*x*); 1 min (*y*). (D) MigA binds to MTs in the absence of EbA. Hyphae of the SRM125 (*alcA$_{(p)}$::mCherry::tubA*, *migA::eGFP*, Δ*ebA*) strain were grown as described. [Exposure time 450–490 nm, 500 ms; 538–562 nm, 500 ms; maximum projection of a 1.82-µm deconvolved *z*-stack. Deconvolution was performed with Zen 2012 Blue Edition v1.20 (Zeiss, Jena, Germany)]. Scale bar: 2 µm. (E) MigA predominantly localizes to the MT plus end in the presence of EbA (arrowheads). Hyphae of the SRM22 (*alcA$_{(p)}$::mCherry::tubA*, *migA::eGFP*) strain were grown as described (exposure time 450–490 nm, 600 ms; 538–562 nm, 500 ms). Scale bar: 2 µm. (F) Confocal scanning image of the interaction of MigA and TubA. Hyphae of the strain SRM105 (*alcA$_{(p)}$::YFPC::migA*, *alcA$_{(p)}$::YFPN::tubA*) were grown as described (frame accumulation, 2; line average, 16; AOTF 514, 25%; gain, 900 V; offset, –0.2; scan speed, 1000 Hz; emission bandwidth, 522 nm–648 nm). Scale bar: 5 µm. CT, C-terminus.

(Su et al., 1995; for a review of Eb1 proteins, see Tirnauer and Bierer, 2000). The APC–Eb1 interaction has been proposed to play a crucial role in chromosomal stability because it is necessary for the physical interaction between MT plus ends and chromosomal kinetochores during mitosis (Fodde et al., 2001).

Because MigA is more closely related to APC than Kar9 is to APC (Fig. 1B), it is possible that this potentially evolutionarily developed mechanism and the influence on cell-end markers is also conserved in human cells. Indeed, MigA and APC share several MT-associated functions. In the absence of the MT cytoskeleton,

Journal of Cell Science (2015) 128, 3569-3582 doi:10.1242/jcs.169094

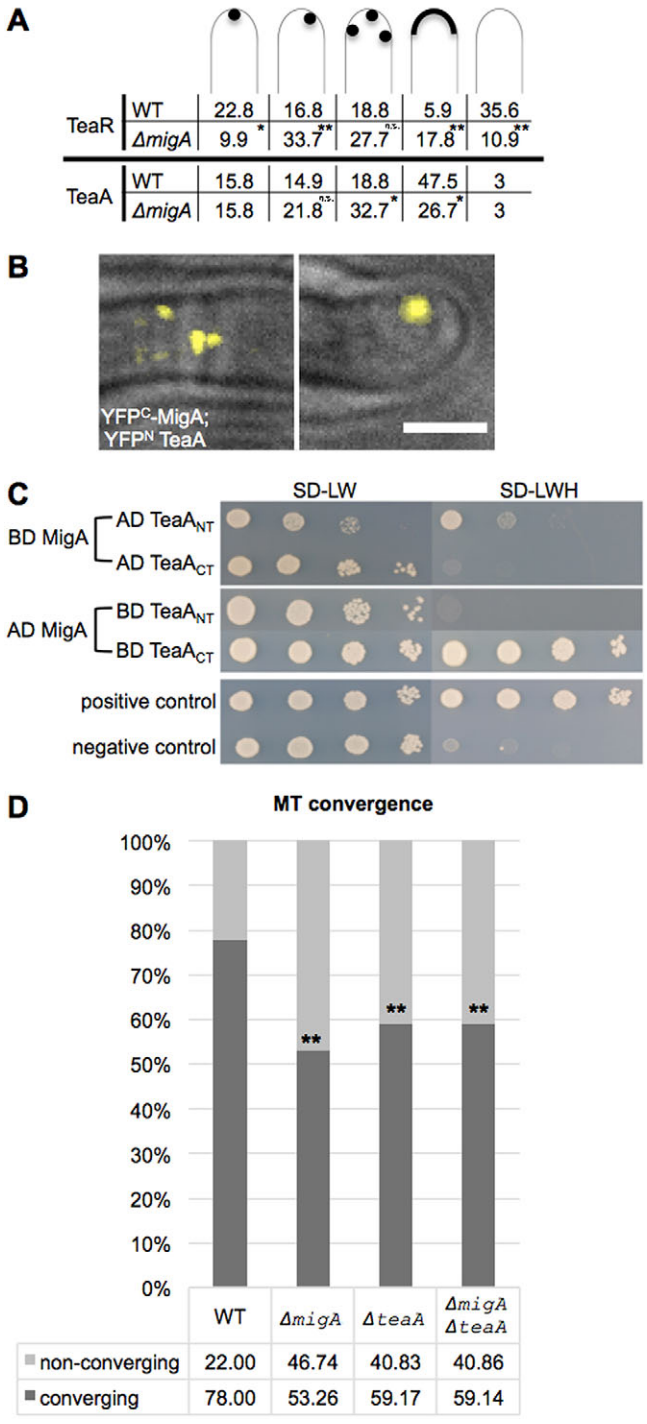

Fig. 6. Role of MigA in cell-end marker positioning. (A) MigA affects positioning of the cell-end marker proteins TeaA and TeaR. Hyphae of the wild-type (WT) strain SNT173 (*eGFP::teaR, mRFP1.2::teaA*) and strain SRM16 (Δ*migA, eGFP::teaR, mRFP1.2::teaA*) were grown as described, and localization of TeaA and TeaR were determined according to the indicated pattern [$n_{(WT)}$=101, $n_{(\Delta migA)}$=101; data in percent; **P*<0.05; ***P*<0.01; a two-tailed Z-test was applied]. (B) Confocal scanning image of the interaction of MigA and TeaA at a prominent point at the hyphal tip. Hyphae of the strain SRM18 (*alcA$_{(p)}$::YFPC::migA*, *alcA$_{(p)}$::YFPN::teaA*) were grown as described (frame accumulation, 2; line average, 8; AOTF 514, 25%; gain, 900 V; offset, −0.2; scan speed, 1000 Hz; emission bandwidth, 522–648 nm; maximum projection of a 5.22-µm *z*-stack). Scale bar: 2 µm. (C) Yeast two-hybrid analysis of MigA and TeaA. Positive and negative controls as provided in the Matchmaker™ Gold Yeast Two-Hybrid System by Clontech Laboratories. Dilution series of respective strains were grown on selective dropout leucine and tryptophan (SD-LW) and selective dropout leucine, tryptophan and histidine (SD-LWH) at 30°C for 3 days. (D) Frequency of MT convergence in wild-type (SRM164), Δ*migA* (SRM166a), Δ*teaA* (SRM168) and Δ*migA* Δ*teaA* (SRM173) strains. eGFP-labeled KipA under the control of the *alcA* promoter was used to visualize MT plus ends. Respective strains were grown as described, and time-lapse images were taken every 378 ms (exposure time 450–490 nm, 200 ms). Trajectories of eGFP–KipA signals in growing tips of respective strains were imaged until fluorescence was depleted. The point where signals attached for the first time to the membrane was monitored, and the distance from that point to the exact center of the hyphal tip was measured. Signals moving along the membrane were set to zero. The number of converging MTs in Δ*migA* (*P*=0), Δ*teaA* (*P*=0.00084) and Δ*migA* Δ*teaA* (*P*=0.00138) strains was significantly lower in comparison to the wild type at *P*<0.01 (two-tailed Z-test). By contrast, the number of converging MTs between the deletion strains did not differ significantly at *P*<0.1 (Δ*migA* to Δ*teaA*, *P*=0.33706; Δ*migA* to Δ*migA* Δ*teaA*, *P*=0.0.41794; Δ*teaA* to Δ*migA* Δ*teaA*, *P*=0.0.9442). In comparison to the wild type (78%), less MTs converge at one point in Δ*migA* (53.26%), Δ*teaA* (59.17%) and Δ*migA* Δ*teaA* (59.14%) strains [WT, $n_{(cells)}$=27, $n_{(MT)}$=150; Δ*migA*, $n_{(cells)}$=15, $n_{(MT)}$=184; Δ*teaA*, $n_{(cells)}$=15, $n_{(MT)}$=120; Δ*migA* Δ*teaA*, $n_{(cells)}$=25, $n_{(MT)}$=93]. AD, activating domain; BD, binding domain; CT, C-terminus; NT, N-terminus. **P*>0.05; ***P*>0.01.

MigA localizes in cortical clusters. A similar localization is known for APC, which accumulates at the cortex, at the very periphery of actively extending membranes (Barth et al., 2002; Barth et al., 1997; Näthke et al., 1996). APC-deficient neuronal cells have a highly disturbed cytoskeleton (Chen et al., 2011), which, with a high number of non-converging MTs, is also true for *A. nidulans migA*-deletion strains. Furthermore, APC and MigA are transported to the MT plus end in an Eb1-dependent manner, although they both bind to tubulin autonomously as well (Deka et al., 1998). It is also reported that APC partially localizes at the basal cortex and that passing MT plus ends pause at the APC puncta. Therefore, APC has been proposed as a template that guides MT network formation (Reilein et al., 2005). This behavior resembles the mechanism described here, where MigA interacts with the cell-end marker TeaA to ensure docking of MTs to the cell cortex.

The interplay between the actin and the MT cytoskeletons is a key step in many cellular processes. Although many open questions remain, the comparative analysis of key components in different organisms helps to develop a general picture.

MATERIALS AND METHODS

Strains, plasmids and culture conditions

Supplemented minimal medium for *A. nidulans* was prepared as described previously, and standard strain construction procedures were used (Takeshita et al., 2008). *A. nidulans* strains used in this study are listed in supplementary material Table S1. The *S. cerevisiae* strains AH109 and Y187 (Clontech) were used for yeast two-hybrid interaction studies. *S. cerevisiae* cells were grown in yeast peptone dextrose adenine (YPDA) complete medium, or on minimal medium (synthetic dropout) supplemented with the dropout-mix needed for selection, as described in the Clontech Matchmaker™ GAL4 Two-Hybrid System 3 Manual (http://www.clontech.com). *S. cerevisiae* strains used in this study are listed in supplementary material Table S2. Standard laboratory *Escherichia coli* strains (Top 10F′) were used. Oligonucleotides are listed in supplementary material Table S3, and plasmids in supplementary material Table S4.

Molecular techniques

Standard DNA transformation procedures were used for *A. nidulans*, *S. cerevisiae* and *E. coli*. For PCR experiments, standard protocols were applied using a personal Cycler (Biometra, Göttingen, Germany) for the reaction cycles. DNA sequencing was performed by a commercial company (MWG Biotech, Ebersberg, Germany). DNA analyses and Southern

Journal of Cell Science (2015) 128, 3569-3582 doi:10.1242/jcs.169094

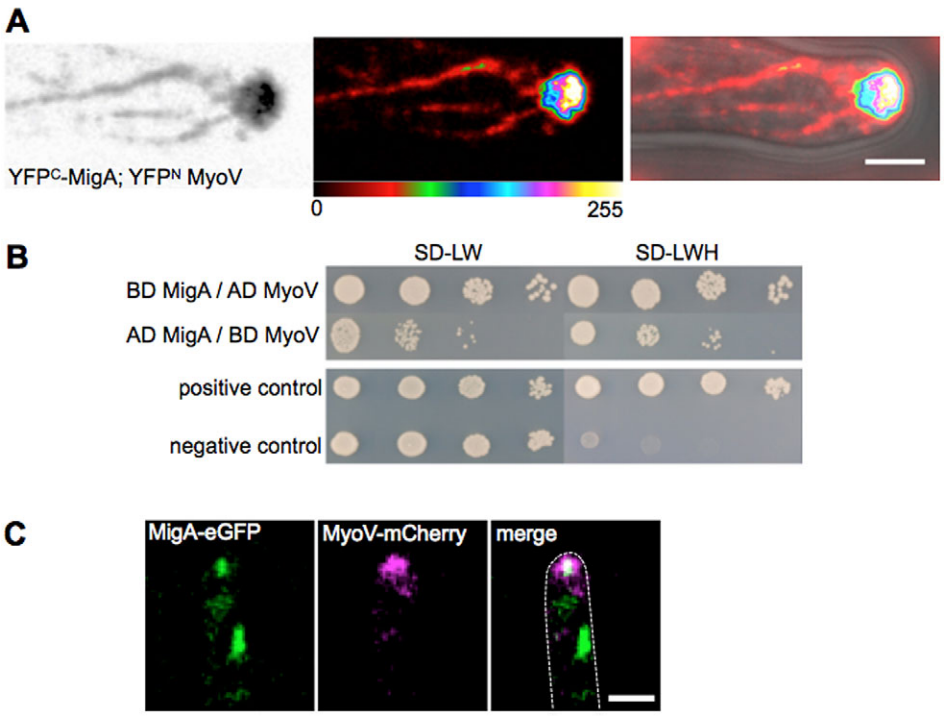

Fig. 7. MigA interacts with the class-V myosin MyoE. (A) Left, confocal scanning image of BiFC of MigA and MyoE at the hyphal tip and along filamentous structures in distal parts of the hyphae. False color heat map (middle) shows fluorescence intensities as a color scheme. Hyphae of the strain SRM17 (*alcA$_{(p)}$::YFPC::migA*, *alcA$_{(p)}$::YFPN::myoE*) were grown as described (frame accumulation, 2; line average, 6; AOTF 514, 20%; gain, 900 V; offset, −0.2; scan speed, 1000 Hz; emission bandwidth, 522–658 nm; maximum projection of a 1.38-µm *z*-stack). Scale bar: 2 µm. (B) Yeast two-hybrid analysis of MigA and MyoE. Positive and negative controls as provided in the Matchmaker™ Gold Yeast Two-Hybrid System by Clontech Laboratories. Dilution series of the indicated strains were grown on selective dropout leucine and tryptophan (SD-LW) and selective dropout leucine, tryptophan and histidine (SD-LWH) at 30°C for 3 days. (C) Colocalization of MigA and MyoE at the hyphal tip. Hyphae of SRM192 (*migA::eGFP*; *myoE::TGACTA::mCherry*) strain were grown as described (exposure time 450–490 nm, 400 ms; 538–562 nm, 500 ms). Scale bar: 2 µm. AD, activating domain; BD, binding domain.

hybridizations were performed as described previously by Sambrook and Russel (1999).

Yeast two-hybrid analysis

Screening for an interaction of MigA with other proteins was performed according to the Matchmaker™ GAL4 Two-Hybrid System 3 Manual (Clontech). Plasmids harboring the *migA* open reading Frame (ORF) were generated by using PCR amplification from genomic DNA (strain TN02A3), introducing *Sfi*I and *EcoR*I restriction sites (primers, KarAFull_Y2HSfiI and KarAFull_Y2HEcoRI) for subsequent ligation into pGBKT7 (Clontech), and *EcoR*I and *Xho*I sites (primers, FullKarA_EcoRIF and FullKarA_XhoIR) for ligation into pGADT7-Rec (Clontech), yielding pRM32 and pRM36, respectively. The C-terminal region of *migA* was amplified by using PCR from cDNA (strain TN02A3)

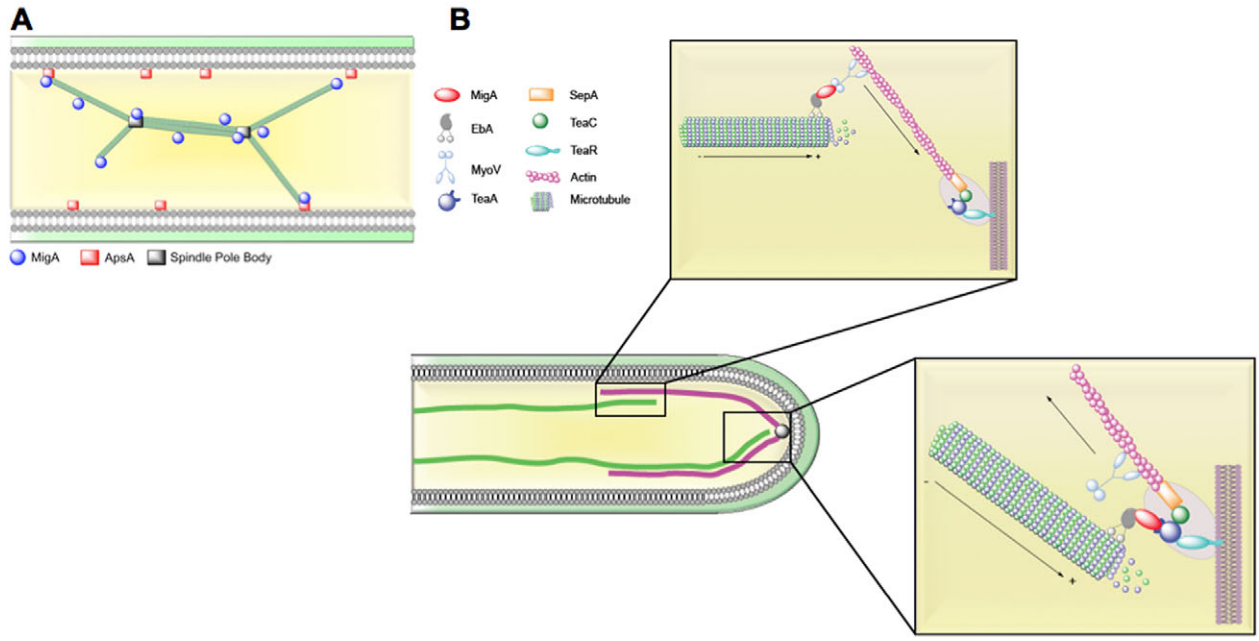

Fig. 8. Model of the MigA pathway. (A) During mitosis, MigA localizes dynamically to both spindle poles and along the mitotic spindle. From spindle pole bodies, MigA is loaded onto astral MTs and transported towards the MT plus ends. At the plasma membrane, MigA facilitates the interaction between astral MTs and ApsA. This mechanism is predominantly important during early stages of mitosis. (B) During interphase, MTs are growing towards the hyphal apex. MigA is able to bind to TubA independently, is transported to the MT plus end in an EbA-dependent manner and reaches the hyphal tip. In the tip region, MigA interacts with MyoE, which drags MigA, and thus the bound MT, along the actin filaments towards the cell-end marker complex. Once at the cortex, MigA interacts with the cell-end marker TeaA and thus anchors the MT for a short time to the polarization site. The model was created with ChemBioDraw Ultra (PerkinElmer, Cambridge).

Journal of Cell Science (2015) 128, 3569-3582 doi:10.1242/jcs.169094

and subsequently ligated into pGADT7-Rec using *Nde*I and *EcoR*I restriction sites (primers, KarACT_Y2HNdeF and KarAFull_Y2HEcoRI) resulting in pRM27. pGBKT7 and pGADT7-Rec with the N-terminal part of *apsA* were generated by using PCR amplification (primers, ApsA_Y2HN_NdeI and ApsA_Y2HN_BamHI) from cDNA (strain TN02A3) and subsequent ligation into the respective vectors through *Nde*I and *BamH*I sites. The same approach was applied for *tubA* (primers, TubA_Y2H_NdeI_fw and TubA_Y2H_BamHI_r), *ebA* (primers, EBA_Y2H_NdeI_for and EBA_Y2H_EcoR_rev) and *myoE* (primers, MyoV_NdeI and MyoV_EcoRI).

In order to generate a plasmid with the mutated SxIP motif ($MigA_{CT}^{\Delta 873–876}$), pRM27 was mutagenized. In a PCR with *Pfu* polymerase and 5′-phosphorylated oligonucleotides flanking the coding region (primers, MigACT_Eb1Mut_fw and MigACT_Eb1Mut_rv), a linear fragment was amplified. The complete reaction was digested with *Dpn*I to cut all methylated original vector molecules, and then ligated. The final plasmid (pRM104) was partially sequenced to confirm the deletion.

Strains AH109 and Y187 were transformed using the lithium chloride method, and transformants were selected on selective synthetic dropout medium as described in the Matchmaker™ GAL4 Two-Hybrid System 3 manual. Expression of all constructs was verified by western blotting (except for AD $MigA_{CT}^{\Delta 873–876}$), and appropriate tests for self-activation were performed (supplementary material Fig. S3C).

Tagging with eGFP and gene deletion

MigA was tagged at the C-terminal end with eGFP. The 1-kb C-terminal region of *migA* was PCR amplified with genomic DNA (strain SO451) with the primer pair KarA_P4 and KarA_P6, and the 1-kb terminator region of the gene with primer pair KarA_P5 and KarA_P8. A fragment of the *eGFP::pyrG* cassette was amplified from pFNO3 using primer pair GA_linker and pyrG_cas_rev. The three fragments were fused together in a subsequent fusion PCR (Nayak et al., 2006) with primer pair KarA_P4 and KarA_P7. In order to introduce a C-terminal mEosFPthermo tag, we amplified the mEosFPthermo construct with primer pair Linker_mIRIS_fwd and IRIS_Linker_rev, the *pyrG* fragment from pFNO3 with primer pair pyrG_cas_for and pyrG_cas_rev and fused together in a fusion PCR with primer pair GA_linker and pyrG_cas_rev. The *mEosFPthermo::pyrG* fragment was also fused to the C-terminal and right border of *migA*, as described previously. The resulting *migA::mEosFPthermo::pyrG* cassette was subcloned into cloning vector pJet1.2 (Fermentas), resulting in pRM35. In order to generate a construct of MigA with a mutated SxIP motif ($MigA^{\Delta 873–876}$), pRM35 was mutagenized in the same way as pRM104 was generated, resulting in pRM105.

The $migA^{\Delta NT}$*::eGFP::pyrG* construct was generated by amplifying the promoter region with KarA_P3 and MigA_P12, the Kar9 domain with primer pair MigA_P11 and MigA_P10. In a subsequent fusion PCR with primer pair KarA_P2 and KarA_P7, the obtained fragments were fused together with the previously described *eGFP::pyrG* cassette and right border. Similarly, the $migA^{\Delta kar9}$*::eGFP::pyrG* was generated by amplifying the promoter and N-terminal region of *migA* with primer pair KarA_P3 and MigA_P9. In the subsequent fusion PCR with primer pair KarA_P2 and KarA_P7, the fragment was fused together with the *eGFP::pyrG* cassette and right border.

In order to tag MyoE at the C-terminus with mCherry and to insert a modified stop codon between the coding sequence of *myoE* and *mCherry*, again fusion PCR was used. The 1-kb C-terminal region of *myoE* was PCR amplified with genomic DNA (strain SO451) with the primer pair MyoV_P1 and MyoV_P2_TGACTA, and the 1-kb terminator region of the gene with primer pair MyoV_P3 and MyoV_RB_rev. A fragment of the *mCherry-pyrG* cassette was also amplified using primer pair GA_linker and pyrG_cas_rev. The three fragments were fused together in a subsequent fusion PCR (Nayak et al., 2006) with primer pair MyoV_nested_for and MyoV_nested_rev. The resulting *myoE::TGACTA::mCherry::pyrG* cassette was subcloned into pJet1.2 (Fermentas). Insertion of the modified stop codon was confirmed by sequencing (MWG Biotech, Ebersberg, Germany).

PCR products were transformed into uridine- and uracil-auxotrophic *A. nidulans ΔnkuA* strain SO451, in order to increase the frequency of homologous integration.

For tagging of MigA at the N-terminus, the 1-kb N-terminal region of the gene was amplified from genomic DNA (strain TN02A3) with primer pair KarA_750bp_for and KarA_750bp_rev, digested with *Asc*I and *Pac*I, and ligated into pCMB17apx, yielding pRM6. The same approach was applied for ApsA (primers, ApsA_1kb_AscI and ApsA_1kb_PacI) and MyoE (primers, AN8862_for_AscI and AN8862_rev_PacI), and then ligated into pDV7, pSH44, pMCB17apx and pJR1, respectively. The plasmids were transformed into the *ΔnkuA* strain TN02A3.

To delete *migA*, the 1-kb promoter region of the gene was amplified with primers KarA_P1 and KarA_P3. A fragment of the *pyrG* marker cassette was amplified with primers pyrG_cas_for and pyrG_cas_rev. PCR products of the promoter region, *pyrG,* and the terminator region amplified using KarA_P5 and KarA_P8 were fused together using fusion PCR with primer pair KarA_P2 and KarA_P7. The PCR products were transformed into the *ΔnkuA* strain SO451. Knockout cassettes were also obtained from the Fungal Genetic Stock Center (FGSC, http://www.fgsc.net/Aspergillus/KO_Cassettes.htm). Amplification of the FGSC *migA* deletion cassette using PCR was performed with primer pair FGSC_KarA_LB_for and FGSC_KarA_RB_rev, the *teaA* deletion cassette with primer pair TeaA_nested_for and TeaA_nested_rev, and the *myoE*-deletion cassette with primer pair FGSC_dMyoVnes_fw and FGSC_dMyoVnes_r. The deletion cassettes were transformed into *ΔnkuA* strains SO451 and TN02A3. The primary transformants were screened with a microscope and PCR to check for correct integration of the eGFP tagging or deletion cassette. Integration events were confirmed by Southern blotting.

Light and fluorescence microscopy

Live-cell imaging of germlings and young hyphae

Up to 4×10^4 spores were grown on 170±5 µm high-precision microscope cover glasses (Roth, Karlsruhe, Germany) in 0.5 ml minimal medium+2% glycerol and appropriate selection markers. Cells were incubated for 12 to 14 h at 28°C following 2 h at room temperature. Alternatively, for *in vivo* time-lapse microscopy, cells were incubated in 35-mm Fluorodish cell culture chambers from World Precision Instruments (Sarasota, FL) in 2 ml minimal medium+2% glycerol and appropriate selection markers, and an additional 7 ml of medium after overnight incubation. For PALM microscopy, cells were incubated in µ-Slide 8-well glass-bottomed chambers (Ibidi, Thermo Fisher Scientific, Martinsried, Germany).

Conventional fluorescence images were captured at room temperature using a Zeiss Plan-Apochromat 63×1.4NA oil DIC and Zeiss EC Plan-Neofluar 100×1.3NA oil objective attached to a Zeiss AxioImager Z.1 combined with an AxioCamMR. Images were collected and analyzed using AxioVision v4.8.1, Zen 2012 Blue Edition v1.20 (Zeiss, Jena, Germany) and ImageJ 1.48p (National Institutes of Health, MD). Image specifications are indicated in the respective legends.

Confocal images were captured at 21°C using a Leica HCX PL APO 63×1.20W Corr objective attached to a Leica TCS SP5 (DM5000) and conventional photomultiplier tube detectors (Leica, Wetzlar, Germany). If not otherwise stated, the pinhole size was set to 1 AU and a 458/514 nm or 488/561/633 nm Notch filter was used. Images were collected and analyzed using LAS AF v2.6 (Leica, Wetzlar, Germany) and ImageJ 1.48p. Acquisition specifications are indicated in the respective figure legends.

PALM imaging was performed as previously described (N. Takeshita, Karlsruhe, personal communication). Briefly, images were acquired at room temperature on a modified inverted microscope (Axiovert 200, Zeiss) equipped with a high-NA water immersion objective (C-Apochromat, 63×, 1.2NA Zeiss). We employed three solid-state lasers, with wavelengths 561 nm (Cobolt Jive, Cobolt, Solna, Sweden), 473 nm (LSR473-200-T00, Laserlight, Berlin, Germany) and 405 nm (CLASII 405-50, Blue Sky Research, Milpitas, CA) for excitation and photoactivation of the fluorophores. The laser sources were combined through dichroic mirrors (AHF, Tübingen, Germany) and guided through an acousto-optic tunable filter (AOTFnC- 400.650, A-A, Opto-Electronic, Orsay Cedex, France). Cells were incubated for 2 h at 28°C followed by 12 to 14 h at room temperature in a chambered cover glass. The photoconvertible fluorescent proteins were converted from their green- to their red-emitting forms using high intensity 405-nm light for 10 s to preconvert sufficient fluorescent protein molecules, followed by simultaneous illumination with low intensity

(0–50 W/cm^2) 405-nm and 561-nm excitation illumination (20–40 W/cm^2). After passing through the excitation dichroic (z 405/473/561/635, AHF, Tübingen, Germany), fluorescence emission was filtered by a 607/50 band-pass filter (AHF, Tübingen, Germany) and recorded with a back-illuminated EMCCD camera (Ixon Ultra 897, Andor, Belfast, Northern Ireland). Recorded images with MigA clusters were localized in each image frame and single-particle-tracking analysis was applied by using our custom written PALM analysis software, a-livePALM (Li et al., 2013). For single-particle analysis, maximum displacement of 300 nm, memory of two frames (allowed frames to skip) and the minimum trajectory length of five frames were used.

Acknowledgements
We thank Bo Liu (Department of Plant Biology, University of California, Davis, CA) for kindly providing the *A. nidulans ΔebA* strain and Michel O. Steinmetz (Laboratory of Biomolecular Research, Paul Scherrer Institut, Villigen, Switzerland) for advice on Eb1 binding motifs.

Competing interests
The authors declare no competing or financial interests.

Author contributions
R.M. performed almost all experiments and was supported by S.H. PALM experiments were done in collaboration with Y.I., G.U.N. and N.T.R.F. and R.M. designed the experiments. All authors contributed to the writing of the manuscript, but most work was done by R.M. and R.F.

Funding
The work was supported by the Deutsche Forschungsgemeinschaft (DFG) (grant numbers Fi459/13-1, TA819/2-1, FOR1334, to the Centre for Functional Nanostructures); the Baden-Württemberg Stiftung; and Karlsruhe Institute of Technology (KIT) in the context of the Helmholtz STN program. R.M. was a fellow of the 'Landesgraduiertenprogramm' of the state of Baden-Württemberg.

Supplementary material
Supplementary material available online at
http://jcs.biologists.org/lookup/suppl/doi:10.1242/jcs.169094/-/DC1

References
Akhmanova, A. and Steinmetz, M. O. (2010). Microtubule +TIPs at a glance. *J. Cell Sci.* **123**, 3415-3419.
Altschul, S. F., Gish, W., Miller, W., Myers, E. W. and Lipman, D. J. (1990). Basic local alignment search tool. *J. Mol. Biol.* **215**, 403-410.
Arkowitz, R. A. (2011). Polarized growth and movement: how to generate new shapes and structures. *Semin. Cell Dev. Biol.* **22**, 789.
Barth, A. I. M., Pollack, A. L., Altschuler, Y., Mostov, K. E. and Nelson, W. J. (1997). NH2-terminal deletion of beta-catenin results in stable colocalization of mutant beta-catenin with adenomatous polyposis coli protein and altered MDCK cell adhesion. *J. Cell Biol.* **136**, 693-706.
Barth, A. I., Siemers, K. A. and Nelson, W. J. (2002). Dissecting interactions between EB1, microtubules and APC in cortical clusters at the plasma membrane. *J. Cell Sci.* **115**, 1583-1590.
Beach, D. L., Thibodeaux, J., Maddox, P., Yeh, E. and Bloom, K. (2000). The role of the proteins Kar9 and Myo2 in orienting the mitotic spindle of budding yeast. *Curr. Biol.* **10**, 1497-1506.
Behrens, J., Jerchow, B.-A., Würtele, M., Grimm, J., Asbrand, C., Wirtz, R., Kühl, M., Wedlich, D. and Birchmeier, W. (1998). Functional interaction of an axin homolog, conductin, with beta-catenin, APC, and GSK3beta. *Science* **280**, 596-599.
Bloom, K. (2000). It's a kar9ochore to capture microtubules. *Nat. Cell Biol.* **2**, E96-E98.
Carminati, J. L. and Stearns, T. (1997). Microtubules orient the mitotic spindle in yeast through dynein-dependent interactions with the cell cortex. *J. Cell Biol.* **138**, 629-641.
Casamayor, A. and Snyder, M. (2002). Bud-site selection and cell polarity in budding yeast. *Curr. Opin. Microbiol.* **5**, 179-186.
Cerqueira, G. C., Arnaud, M. B., Inglis, D. O., Skrzypek, M. S., Binkley, G., Simison, M., Miyasato, S. R., Binkley, J., Orvis, J., Shah, P. et al. (2013). The Aspergillus Genome Database: multispecies curation and incorporation of RNA-Seq data to improve structural gene annotations. *Nucleic Acids Res.* **42**, D705-D710.
Chen, Y., Tian, X., Kim, W.-Y. and Snider, W. D. (2011). Adenomatous polyposis coli regulates axon arborization and cytoskeleton organization via its N-terminus. *PLoS ONE* **6**, e24335.
Deka, J., Kuhlmann, J. and Müller, O. (1998). A domain within the tumor suppressor protein APC shows very similar biochemical properties as the microtubule-associated protein tau. *Eur. J. Biochem.* **253**, 591-597.
Dent, E. W., Gupton, S. L. and Gertler, F. B. (2011). The growth cone cytoskeleton in axon outgrowth and guidance. *Cold Spring Harb. Perspect. Biol.* **3**.
Enke, C., Zekert, N., Veith, D., Schaaf, C., Konzack, S. and Fischer, R. (2007). Aspergillus nidulans Dis1/XMAP215 protein AlpA localizes to spindle pole bodies and microtubule plus ends and contributes to growth directionality. *Eukaryot. Cell* **6**, 555-562.
Farkasovsky, M. and Kuntzel, H. (2001). Cortical Num1p interacts with the dynein intermediate chain Pac11p and cytoplasmic microtubules in budding yeast. *J. Cell Biol.* **152**, 251-262.
Feierbach, B. and Chang, F. (2001). Roles of the fission yeast formin for3p in cell polarity, actin cable formation and symmetric cell division. *Curr. Biol.* **11**, 1656-1665.
Finn, R. D., Bateman, A., Clements, J., Coggill, P., Eberhardt, R. Y., Eddy, S. R., Heger, A., Hetherington, K., Holm, L., Mistry, J. et al. (2014). Pfam: the protein families database. *Nucleic Acids Res.* **42**, D222-D230.
Fischer, R. and Timberlake, W. E. (1995). Aspergillus nidulans apsA (anucleate primary sterigmata) encodes a coiled-coil protein required for nuclear positioning and completion of asexual development. *J. Cell Biol.* **128**, 485-498.
Fischer, R., Zekert, N. and Takeshita, N. (2008). Polarized growth in fungi – interplay between the cytoskeleton, positional markers and membrane domains. *Mol. Microbol.* **68**, 813-826.
Fodde, R., Kuipers, J., Rosenberg, C., Smits, R., Kielman, M., Gaspar, C., van Es, J. H., Breukel, C., Wiegant, J., Giles, R. H. et al. (2001). Mutations in the APC tumour suppressor gene cause chromosomal instability. *Nat. Cell Biol.* **3**, 433-438.
Freitag, J., Ast, J. and Bölker, M. (2012). Cryptic peroxisomal targeting via alternative splicing and stop codon read-through in fungi. *Nature* **485**, 522-525.
Gasteiger, E., Hoogland, C., Gattiker, A., Duvaud, S., Wilkins, M. R., Appel, R. D. and Bairoch, A. (2005). Protein identification and analysis Tools on the ExPASy server. In *The Proteomics Protocols Handbook* (ed. J. M. Walker), pp. 571-607. Humana Press, New York City.
Groden, J., Thliveris, A. Samowitz, W., Carlson, M., Gelbert, L., Albertsen, H., Joslyn, G., Stevens, J., Spirio, L., Robertsen, M. et al. (1991). Identification and characterization of the familial adenomatous polyposis coli gene. *Cell* **66**, 589-600.
Han, G., Liu, B., Zhang, J., Zuo, W., Morris, N. R. and Xiang, X. (2001). The Aspergillus cytoplasmic dynein heavy chain and NUDF localize to microtubule ends and affect microtubule dynamics. *Curr. Biol.* **11**, 719-724.
Higashitsuji, Y., Herrero, S., Takeshita, N. and Fischer, R. (2009). The cell end marker protein TeaC is involved in growth directionality and septation in Aspergillus nidulans. *Eukaryot. Cell* **8**, 957-967.
Honnappa, S., Gouveia, S. M., Weisbrich, A., Damberger, F. F., Bhavesh, N. S., Jawhar, H., Grigoriev, I., van Rijssel, F. J. A., Buey, R. M., Lawera, A. et al. (2009). An EB1-binding motif acts as a microtubule tip localization signal. *Cell* **138**, 366-376.
Hwang, E., Kusch, J., Barral, Y. and Huffaker, T. C. (2003). Spindle orientation in Saccharomyces cerevisiae depends on the transport of microtubule ends along polarized actin cables. *J. Cell Biol.* **161**, 483-488.
Ishitsuka, Y., Nienhaus, K. and Nienhaus, G. U. (2014). Photoactivatable fluorescent proteins for super-resolution microscopy. *Methods Mol. Biol.* **1148**, 239-260.
Kerppola, T. K. (2008). Bimolecular fluorescence complementation (BiFC) analysis as a probe of protein interactions in living cells. *Annu. Rev. Biophys.* **37**, 465-487.
Konzack, S., Rischitor, P. E., Enke, C. and Fischer, R. (2005). The role of the kinesin motor KipA in microtubule organization and polarized growth of Aspergillus nidulans. *Mol. Biol. Cell* **16**, 497-506.
Lee, L., Tirnauer, J. S., Li, J., Schuyler, S. C., Liu, J. Y. and Pellman, D. (2000). Positioning of the mitotic spindle by a cortical-microtubule capture mechanism. *Science* **287**, 2260-2262.
Li, Y., Ishitsuka, Y., Hedde, P. N. and Nienhaus, G. U. (2013). Fast and efficient molecule detection in localization-based super-resolution microscopy by parallel adaptive histogram equalization. *ACS Nano.* **7**, 5207-5214.
Liakopoulos, D., Kusch, J., Grava, S., Vogel, J. and Barral, Y. (2003). Asymmetric loading of Kar9 onto spindle poles and microtubules ensures proper spindle alignment. *Cell* **112**, 561-574.
Lu, B., Roegiers, F., Jan, L. Y. and Jan, Y. N. (2001). Adherens junctions inhibit asymmetric division in the Drosophila epithelium. *Nature* **409**, 522-525.
Maekawa, H., Usui, T., Knop, M. and Schiebel, E. (2003). Yeast Cdk1 translocates to the plus end of cytoplasmic microtubules to regulate bud cortex interactions. *EMBO J.* **22**, 438-449.
Martin, S. G. and Arkowitz, R. A. (2014). Cell polarization in budding and fission yeasts. *FEMS Microbiol. Rev.* **38**, 228-253.
Mata, J. and Nurse, P. (1997). tea1 and the microtubular cytoskeleton are important for generating global spatial order within the fission yeast cell. *Cell* **89**, 939-949.
Miller, R. K. and Rose, M. D. (1998). Kar9p is a novel cortical protein required for cytoplasmic microtubule orientation in yeast. *J. Cell Biol.* **140**, 377-390.

Miller, R. K., Cheng, S.-C. and Rose, M. D. (2000). Bim1p/Yeb1p mediates the Kar9p-dependent cortical attachment of cytoplasmic microtubules. *Mol. Biol. Cell* **11**, 2949-2959.
Moore, J. K. and Miller, R. K. (2007). The cyclin-dependent kinase Cdc28p regulates multiple aspects of Kar9p function in yeast. *Mol. Biol. Cell* **18**, 1187-1202.
Munemitsu, S., Souza, B., Müller, O., Albert, I., Rubinfeld, B. and Polakis, P. (1994). The APC gene product associates with microtubules in vivo and promotes their assembly in vitro. *Cancer Res.* **54**, 3676-3681.
Näthke, I. S., Adams, C. L., Polakis, P., Sellin, J. H. and Nelson, W. J. (1996). The adenomatous polyposis coli tumor suppressor protein localizes to plasma membrane sites involved in active cell migration. *J. Cell Biol.* **134**, 165-179.
Nayak, T., Szewczyk, E., Oakley, E. C., Osmani, A., Ukil, L., Murray, S. L., Hynes, M. J., Osmani, M. J., Osmani, S. A. and Oakley, B. R. (2006). A versatile and efficient gene-targeting system for Aspergillus nidulans. *Genetics* **172**, 1557-1566.
Pantazopoulou, A., Pinar, M., Xiang, X. and Peñalva, M. A. (2014). Maturation of late Golgi cisternae into RabERAB11 exocytic post-Golgi carriers visualized in vivo. *Mol. Biol. Cell* **25**, 2428-2443.
Patterson, G., Davidson, M., Manley, S. and Lippincott-Schwartz, J. (2010). Superresolution imaging using single-molecule localization. *Annu. Rev. Phys. Chem.* **61**, 345-367.
Peñalva, M. (2010). Endocytosis in filamentous fungi: Cinderella gets her reward. *Curr. Opin. Microbiol.* **13**, 684-692.
Pereira, G., Tanaka, T. U., Nasmyth, K. and Schiebel, E. (2001). Modes of spindle pole body inheritance and segregation of the Bfa1p-Bub2p checkpoint protein complex. *EMBO J.* **20**, 6359-6370.
Philips, J. and Herskowitz, I. (1998). Identification of Kel1p, a Kelch domain-containing protein involved in cell fusion and morphology in Saccharomyces cerevisiae. *J. Cell Biol.* **143**, 375-389.
Riquelme, M. (2013). Tip growth in filamentous fungi: a road trip to the apex. *Annu. Rev. Microbiol.* **67**, 587-609.
Reilein, A. and Nelson, W. J. (2005). APC is a component of an organizing template for cortical microtubule networks. *Nat. Cell Biol.* **7**, 463-473.
Sambrook, J. and Russel, D. W. (1999). *Molecular Cloning: A Laboratory Manual*. Cold Spring Harbor, NY: Cold Spring Harb. Lab. Press.
Schunck, T., Herrero, S. and Fischer, R. (2011). The Aspergillus nidulans CENP-E kinesin KipA is able to dimerize and to move processively along microtubules. *Curr. Genet.* **57**, 335-341.
Snaith, H. A. and Sawin, K. E. (2003). Fission yeast mod5p regulates polarized growth through anchoring of tea1p at cell tips. *Nature* **423**, 647-651.
Snell, V. and Nurse, P. (1994). Genetic analysis of cell morphogenesis in fission yeast - a role for casein kinase II in the establishment of polarized growth. *EMBO J.* **13**, 2066-2074.
Stiebler, A. C., Freitag, J., Schink, K. O., Stehlik, T., Tillmann, B. A. M., Ast, J. and Bölker, M. (2014). Ribosomal readthrough at a short UGA stop codon context triggers dual localization of metabolic enzymes in fungi and animals. *PLoS Genet.* **10**, e1004685.
Su, L. K., Burrell, M., Hill, D. E., Gyuris, J., Brent, R., Wiltshire, R., Trent, J., Vogelstein, B. and Kinzler, K. W. (1995). APC binds to the novel protein EB1. *Cancer Res.* **55**, 2972-2977.
Suelmann, R., Sievers, N., Galetzka, D., Robertson, L., Timberlake, W. E. and Fischer, R. (1998). Increased nuclear traffic chaos in hyphae of Aspergillus nidulans : molecular characterization of apsB and in vivo observation of nuclear behaviour. *Mol. Microbiol.* **30**, 831-842.
Taheri-Talesh, N., Xiong, Y. and Oakley, B. R. (2012). The functions of myosin II and myosin V homologs in tip growth and septation in Aspergillus nidulans. *PLoS ONE* **7**, e31218.
Takeshita, N., Higashitsuji, Y., Konzack, S. and Fischer, R. (2008). Apical sterol-rich membranes are essential for localizing cell end markers that determine growth directionality in the filamentous fungus Aspergillus nidulans. *Mol. Biol. Cell* **19**, 339-351.
Takeshita, N., Mania, D., Herrero, S., Ishitsuka, Y., Nienhaus, G. U., Podolski, M., Howard, J. and Fischer, R. (2013). The cell-end marker TeaA and the microtubule polymerase AlpA contribute to microtubule guidance at the hyphal tip cortex of Aspergillus nidulans to provide polarity maintenance. *J. Cell Sci.* **126**, 5400-5411.
Takeshita, N., Manck, R., Grün, N., de Vega, S. H. and Fischer, R. (2014). Interdependence of the actin and the microtubule cytoskeleton during fungal growth. *Curr. Opin. Microbiol.* **20**, 34-41.
Tamura, K., Peterson, D., Peterson, N., Stecher, G., Nei, M. and Kumar, S. (2011). MEGA5: Molecular evolutionary genetics analysis using maximum likelihood, evolutionary distance, and maximum parsimony methods. *Mol. Biol. Evol.* **28**, 2731-2739.
Tirnauer, J. S. and Bierer, B. E. (2000). EB1 proteins regulate microtubule dynamics, cell polarity, and chromosome stability. *J. Cell Biol.* **149**, 761-766.
Upadhyay, S. and Shaw, B. D. (2008). The role of actin, fimbrin and endocytosis in growth of hyphae in Aspergillus nidulans. *Mol. Microbiol.* **68**, 690-705.
van der Vaart, B., Manatschal, C., Grigoriev, I., Olieric, V., Gouveia, S. M., Bjelić, S., Demmers, J., Vorobjev, I., Hoogenraad, C. C., Steinmetz, M. O. et al. (2011). SLAIN2 links microtubule plus end-tracking proteins and controls microtubule growth in interphase. *J. Cell Biol.* **193**, 1083-1099.
Wiedenmann, J., Ivanchenko, S., Oswald, F., Schmitt, F., Röcker, C., Salih, A., Spindler, K.-D. and Nienhaus, G. U. (2004). EosFP, a fluorescent marker protein with UV-inducible green-to-red fluorescence conversion. *Proc. Natl. Acad. Sci.* **101**, 15905-15910.
Wiedenmann, J., Gayda, S., Adam, V., Oswald, F., Nienhaus, K., Bourgeois, D. and Nienhaus, G. U. (2011). From EosFP to mIrisFP: Structure-based development of advanced photoactivatable marker proteins of the GFP-family. *J. Biophotonics* **4**, 377-390.
Wolf, E., Kim, P. S. and Berger, B. (1997). MultiCoil: a program for predicting two- and three-stranded coiled coils. *Protein Sci.* **6**, 1179-1189.
Yin, H., Pruyne, D., Huffaker, T. C. and Bretscher, A. (2000). Myosin V orientates the mitotic spindle in yeast. *Nature* **406**, 1013-1015.
Zekert, N. and Fischer, R. (2009). The Aspergillus nidulans kinesin-3 UncA motor moves vesicles along a subpopulation of microtubules. *Mol. Biol. Cell* **20**, 673-684.
Zeng, C. J. T., Kim, H.-R., Vargas Arispuro, I., Kim, J.-M., Huang, A.-C. and Liu, B. (2014). Microtubule plus end-tracking proteins play critical roles in directional growth of hyphae by regulating the dynamics of cytoplasmic microtubules in Aspergillus nidulans. *Mol. Microbiol.* **94**, 506-521.
Zhang, J., Tan, K., Wu, X., Chen, G., Sun, J., Reck-Peterson, S. L., Hammer, J. A. and Xiang, X. (2011). Aspergillus myosin-V supports polarized growth in the absence of microtubule-based transport. *PLoS One* **6**, e28575.
Zumbrunn, J., Kinoshita, K., Hyman, A. A. and Näthke, I. S. (2001). Binding of the adenomatous polyposis coli protein to microtubules increases microtubule stability and is regulated by GSK3 beta phosphorylation. *Curr. Biol.* **11**, 44-49.